UNIVERSIDADE FEDERAL DE MINAS GERAIS
PROGRAMA DE PÓS-GRADUAÇÃO EM FÍSICA

Kevin Liu Rodrigues

Synchronization of phase oscillators

BELO HORIZONTE
2021

Kevin Liu Rodrigues

Synchronization of Phase Oscilators

Tese apresentada ao Programa de Pós-Graduação em Física do Instituto de Ciências Exatas da Universidade Federal de Minas Gerais como requisito parcial para obtenção do título de Doutor em Ciências.

Supervisor: Ronald Dickman

Belo Horizonte

2021

Dados Internacionais de Catalogação na Publicação (CIP)

R696s Rodrigues, Kevin Liu.
Synchronization of phase oscillators / Kevin Liu Rodrigues. – 2021.
77f., enc. : il.

Orientador: Ronald Dickman.
Tese (doutorado) – Universidade Federal de Minas Gerais, Departamento de Física.
Bibliografia: f. 69-71.

1. Osciladores acoplados. 2. Física estatística. 3. Sistemas complexos. 4. Física computacional.
I. Título. II. Dickman, Ronald. III. Universidade Federal de Minas Gerais, Departamento de Física.

CDU – 531.19 (043)

Ficha catalográfica elaborada por Romário Martins Ribeiro – CRB6 3595
Biblioteca Professor Manoel Lopes de Siqueira – Departamento de Física - UFMG

UNIVERSIDADE FEDERAL DE MINAS GERAIS
INSTITUTO DE CIÊNCIAS EXATAS
PROGRAMA DE PÓS-GRADUAÇÃO EM FÍSICA

FOLHA DE APROVAÇÃO

A presente tese, intitulada **"Synchronization of phase oscillators"** de autoria de **KEVIN LIU RODRIGUES** submetida à Comissão Examinadora, abaixo-assinada, foi aprovada para obtenção do grau de **DOUTOR EM CIÊNCIAS**, em vinte e sete de agosto de 2021.

Belo Horizonte, 27 de agosto de 2021.

Prof. Ronald Dickman
Orientador do estudante
Departamento de Física/UFMG

Prof. Kevin Wood
University of Michigan

Prof. Lucas Lages Wardil
Departamento de Física/UFMG

Prof. Daniel Elias Escaff Dixon
Universidad de Los Andes

Prof. Reinaldo Oliveira Vianna
Departamento de Física/UFMG

Documento assinado eletronicamente por **Lucas Lages Wardil**, **Professor do Magistério Superior**, em 01/09/2021, às 10:41, conforme horário oficial de Brasília, com fundamento no art. 5º do Decreto nº 10.543, de 13 de novembro de 2020.

Documento assinado eletronicamente por **Reinaldo Oliveira Vianna**, **Professor do Magistério Superior**, em 01/09/2021, às 13:28, conforme horário oficial de Brasília, com fundamento no art. 5º do Decreto nº 10.543, de 13 de novembro de 2020.

Acknowledgements

I acknowledge the orientation of professor Ronald Dickman, who helped formalize mathematical arguments, select a simulation methodology and more.

I would also like to acknowledge Professor Kevin Wood, from the University of Michigan for hosting me as an invited researcher, providing computational resources as well as insightful conversations.

I acknowledge the partial funding provided by Capes and Cnpq.

Abstract

In this work we extend the investigation of coupled discrete phase oscillators to circular networks with non-global coupling, using analytic approximations and simulation. For the later, the chosen method is an event-driven simulation. Its general implementation allows for the investigation of arbitrary graphs, and is used to investigate small-world networks. At the same time, a mean-field (MF) approximation for small-world networks is introduced, which predicts the stability of travelling waves at positive coupling, where usually the globally synchronized solution would be observed. In the zero disorder limit the MF recovers the mean-field approximation proposed in previous works, but here travelling waves are found to be stable even when the underlying graph has some disorder. The wave solutions compete with global oscillations as well as with each other when there is more than one stable wave number, leading to spontaneous transitions between wave numbers. Finite systems will always be subject to these fluctuations, but larger systems are more robust since noise becomes smaller relative to wave period and amplitude.

Preliminary simulations and scaling analyses indicated that wave solutions did not lose stability if interaction range and system size are increased in the same proportion, a property which is captured by the MF approximation. To further probe its validity, we tested other predictions such as wave stability in the presence of disorder, the later introduced through rewiring the base graph. Another finding is that the speed of propagation of such waves should increase with increasing natural frequencies, which is verified in simulation.

Keywords: Dissertation, Doctoral thesis, Dynamical systems, Statistical physics, Couple oscillators, Networks.

Resumo

Neste trabalho estendemos o estudo de sistemas de osciladores acoplados para redes circulares de acoplamento não global utilizando modelagem matemática e simulações. O método simulacional é do tipo "event driven", e a sua implementação genérica permitiu a investigação de grafos de conectividade arbitrários de modo que redes de mundo pequeno também puderam ser investigadas. Também desenvolvemos uma teoria de campo médio para descrever o comportamento coletivo dos osciladores acoplados nessas redes de mundo pequeno, que prevê a estabilidade de ondas viajantes em regimes de acoplamento positivo. Em geral nessas condições se observa uma sincronia global entre osciladores, mas o alcance não global das interações permite a sobrevivência de tais estados. No entanto, a descrição também prevê a estabilidade de ondas mesmo quando desordem de alcance global é introduzida no sistema através de um algorítimo de reconexão do grafo subjacente. Nesse regime a solução de ondas viajantes está constantemente competindo com outros estados estáveis, como oscilações globais ou ondas viajantes com número de onda diferente (quando há mais de um número de onda estável). Isso faz com que o sistema nunca atinga propriedades macroscópicas estáveis, mesmo depois de longos tempos. Sistemas finitos sempre estarão sujeitos a esse tipo de regime, com a criação e aniquilação espontânea de números de onda, mas se tornam mais estáveis quando o tamanho do sistema cresce, tornando a intensidade das flutuações nas frentes de onda pequenas em relação a amplitude das ondas.

Inicialmente, as simulações indicaram que soluções de ondas viajantes permanecem estáveis se o tamanho do sistema cresce proporcionalmente ao alcance das interações, uma propriedade que foi capturada pela aproximação de campo médio. Para fortalecer a validade de tal aproximação, algumas de suas previsões foram testadas, como a estabilidade de ondas viajantes na presença de desordem introduzida pelo processo de reconexão. Outro resultado é a modulação da velocidade de propagação das ondas através de vieses macroscópicos introduzidos nas frequências naturais de oscilação das unidades microscópicas do sistema, que também foi verificado em simulação.

Palavras-chave: Dissertação, Tese doutorado, Sistemas dinâmicos, Física estatística, Osciladores acoplados, Redes. brazil

Contents

Introduction

In 1951 the Belousov-Zhabotinsky class of chemical reactions were created for the first time in a laboratory. This feat marked an upheaval in thermodynamics, which had now been shown, experimentally, to be ruled by non-equilibrium dynamics even for long mixing times. This generated for the first time interest in the field of coupled oscillators by the broader scientific community. In the decades that followed, other areas of research independently led to the same interests. In 1958, Norbet Weiner at MIT was looking at power spectra from brain scans and decided that there must be some kind of synchronization amongst coupled, periodically-firing, neurons. Also inspired by many biological rhythms observed in nature, Arthur Winfree published in 1967 a paper on the mathematical modelling of interacting oscillators. Winfree defined a phase oscillator as an abstraction of any system that possesses periodicity. As such, a complicated periodic process inside a living cell could be described by a single real number, between 0 and 2π, and its rate of change. The major simplification comes from the fact that when two such phase oscillators interact, each influences *only* the rate of change in phase of the other. Their trajectories in phase space are assumed to remain closed loops, and thus the only effective change can be modeled as a change in the speed at which they traverse it.

Seven years after Winfree's 1967 paper, the young Japanese scientist Yoshiki Kuramoto recognized what made Winfree's model hard to solve. He proposed a modified version of it, assuming a particular form for the coupling between oscillators. This led to an arguably less realistic model, but one which Kuramoto was cunningly able to solve. This modified version, together with its solution, would later be recognized as the Kuramoto model, becoming one of the major founding stones in the field.

Since then, a plethora of novel coupled oscillator models have been put forward. One class deals with discrete phase oscillators, in which the phase that describes a unit is related to a finite set of possible values. Discrete-phase models are used to describe systems which exhibit markedly distinct states. An example of such a system is interacting neurons, where one can identify the three distinct phases of a neuron as firing, refractory and ready-to-fire.

Another element present in some models is stochasticity in the dynamics, which is deterministic in the Kuramoto model. The element of stochasticity may be included to account for noise, such as in models of open systems that interact with a heat bath.

Here we consider discrete-phase models with three possible phase states, and stochasticity plays a role in the rate of change of the phase state of each unit, being the probability of "jumping" to the next state per unit time. This model was introduced by

Kevin Wood, C. Van den Broeck, R. Kawai and Katja Lindenberg [1], with the main motivation of finding the simplest possible dynamics between phase oscillators that still led to a phase transition to synchrony. Initial investigations focused mainly on square lattices and all-to-all connections, exposing the ubiquity of this type of self-organization. Often times, networks of coupled oscillators observed in nature possess neither of these two. Neurons, fireflies and cardiac cells are all examples of systems that do not operate on lattices or complete-graph networks. One common type of interaction network observed in real systems is a mix between local and global interactions. Various algorithms have been proposed for the generation of such intermediate connectivity graphs, some of which generate small-world networks, characterized by the presence of long-range interactions while preserving strong local clustering.

A particular example for the generation of small-world networks is the Watts-Strogatz algorithm, which randomly breaks connections on an existing graph and re-creates them between random vertices. When applied to certain starting graphs with strong local clustering, the result is a small-world network. Here we investigate how the dynamics of the three-phase oscillator model unfolds on such networks, via simulation and a mean-field analysis.

1 Kuramoto Model

In this chapter we describe the Kuramoto model, its dynamics and self-consistency arguments that allow for a synchronous phase to emerge at some critical coupling. To do this, an order parameter is introduced together with a mean-field (MF) approximation. The stability analysis of the solutions of the Kuramoto model took decades to develop and led to some very anti intuitive findings, such as the fact that the disordered phase for weak coupling is not stable, but neutrally stable, and is related to Landau damping in plasma physics. Nonetheless, the two branches of solutions identified in Kuramoto's initial work don't require solving the original set of equations, but rather rely on assuming macroscopic behaviors for the system and tracing back what implications they have for the microscopic dynamics. This feedback from macro to micro is central to Kuramoto's self-consistency arguments, which helped popularize his model by lowering the barrier of entry to understanding synchronization in complex systems. Much of the discussion developed in this section are reproductions from the notes of da Fonseca Abud [2].

1.1 Definition

The Kuramoto model consists of a collection of phase oscillators ("units") which are all coupled to each other. We start with a collection of N oscillators and then take the continuous limit with $N \to \infty$. Each unit j at time t is described by its phase $\theta_j(t)$ and its natural frequency ω_j, which is its rate of change in phase in isolation, and is assumed to be constant. The natural frequencies $\boldsymbol{\omega} \equiv \{\omega_1, \ldots, \omega_N\}$ are assumed to follow some frequency distribution $\boldsymbol{\omega} \sim g(\boldsymbol{\omega})$ which is symmetric about some frequency $\bar{\omega}$, and unimodal. While the rate of change of an isolated unit is time independent, the coupling between oscillators makes $\dot{\theta_j}$ a function of the entire phase configuration $\boldsymbol{\theta}(t) \equiv \{\theta_1(t), \ldots, \theta_N(t)\}$.

The biologically inspired Winfree model states that, at every instant, each oscillator sends a signal of strength $P(\theta)$ and responds by adjusting its own phase proportionally to $Q(\theta)$ when receiving signals from other units, which is captured in the equation:

$$\dot{\theta_j} = \omega_j + \frac{1}{N}\sum_{k}^{N} P(\theta_k)Q(\theta_j), \qquad j = 1, ..., N \tag{1.1}$$

In the special case where the product $P(\theta_k)Q(\theta_j)$ depends only on the phase difference between oscillators j and k, the product inside the summation can be written as a single function called the kernel F: $P(\Delta\theta)Q(\Delta\theta) \equiv F(\Delta\theta)$. If furthermore the kernel is proportional to the sine function, then Winfree's equation (1.1) becomes the Kuramoto model:

$$\dot{\theta}_j = \omega_j + \frac{K}{N}\sum_k^N \sin(\theta_k - \theta_j), \qquad j = 1, ..., N \tag{1.2}$$

where $K \geq 0$ is a real constant which describes the coupling strength between any pair of oscillators.

1.2 Mean-field and order parameter

To determine if the microscopic collection of phases represents a synchronized macro state, we introduce the Kuramoto order parameter R. It maps a phase configuration $\boldsymbol{\theta}$ to a magnitude by representing the phases as complex numbers on the unit circle and performing a complex summation:

$$R(\boldsymbol{\theta})e^{i\phi(\boldsymbol{\theta})} \equiv \frac{1}{N}\sum_k^N e^{i\theta_k(t)} \tag{1.3}$$

where $i = \sqrt{-1}$ and $\phi(\boldsymbol{\theta}) \in [0, 2\pi)$ is the resulting polar angle of the summation. Thus $R(\boldsymbol{\theta}) \in [0, 1]$ determines the overall macroscopic alignment between phases. With this definition the equations of motion can be re-written as:

$$\begin{aligned}
\dot{\theta}_j &= \omega_j + \frac{K}{N}\sum_k^N \sin(\theta_k - \theta_j) \\
&= \omega_j + K\,\mathrm{Im}\left(\frac{1}{N}\sum_k^N e^{i(\theta_k - \theta_j)}\right) \\
&= \omega_j + KR(\boldsymbol{\theta})\,\mathrm{Im}\left(e^{i(\phi(\boldsymbol{\theta}) - \theta_j)}\right)
\end{aligned}$$

$$\dot{\theta}_j = \omega_j + KR(\boldsymbol{\theta})\sin(\phi(\boldsymbol{\theta}) - \theta_j) \tag{1.4}$$

We see that the equations of motion are now written in terms of the mean fields $R(\boldsymbol{\theta})$ and $\phi(\boldsymbol{\theta})$. In particular, if the fields are constant ($\dot{R} = \dot{\phi} = 0$) then the equations of motion become decoupled and can be solved.

The collective oscillations observed in real systems tell us that the macroscopic steady-state solution of stable synchronized oscillations should indeed have constant $R > 0$ while ϕ increases linearly with time (the system rotates synchronously with constant phase speed). Thus, $\phi = \Omega t$ and both R and Ω are constant. Even though ϕ itself is not constant, it turns out that the rotational symmetry of equation (1.4) allows us to decouple the equations by moving to a rotating frame of reference with the following substitution:

$$\begin{aligned} \forall j: \quad \theta_j(t) &= \varphi_j(t) + \Omega t \\ &\Downarrow \\ \dot{\varphi}_j &= (\omega_j - \Omega) - KR\sin(\varphi_j) \end{aligned} \tag{1.5}$$

Another macroscopic behavior observed in nature is the more trivial one, with no synchronization at all. In this state the phase configuration is evenly distributed over all possible values, leading to constant $R = 0$, and is also described by equation (1.5). Inspection of this equation shows that when $|\omega_j - \Omega| \leq KR$ there is some phase value for which $\dot{\varphi}_j = 0$, and thus oscillators become phase-locked when attaining this value. When $|\omega_j - \Omega| > KR$, the φ_j can never stop varying and will permanently drift. For a synchronized solution we then expect two groups of oscillators:

- **Phase-Locked** $|\omega_j - \Omega| \leq KR$: A group of oscillators with natural frequencies close enough to Ω will become phase locked and sync.
- **Drifting** $|\omega_j - \Omega| > KR$: Remaining oscillators with frequencies too far from the generated mean-field will remain drifting ahead or behind the synced group.

Since we postulate that R is time independent, self-consistency requires that the phase distribution generated by the drifting oscillators must be stationary, otherwise R would not be constant.

1.3 Continuous Limit

In the continuous limit $N \to \infty$, the distribution of oscillator phases can be written as the joint probability density in phases φ and natural frequencies ω as:

$$P(\varphi_j, \omega_j, t) \to p(\varphi, \omega, t) \qquad \varphi \in [-\pi, \pi) \qquad \omega \in (-\infty, \infty)$$

For given values of φ and ω, the evolution follows

$$\dot{\varphi} = (\omega - \Omega) - KR\sin(\varphi). \tag{1.6}$$

The density of oscillators with phase φ is then given by the marginal distribution:

$$n(\varphi) = \int_{-\infty}^{\infty} p(\varphi, \omega, t) d\omega$$

which by the definition of conditional probability gives:

$$n(\varphi) = \int_{-\infty}^{\infty} p(\varphi|\omega) g(\omega) d\omega$$

where $p(\varphi|\omega)$ is the conditional probability density that an oscillator with given natural frequency ω has phase $\varphi \equiv \varphi(t)$ at time t.

By using the subscripts L and D to indicate the *phase-locked* and *drifting* groups, we get the expression for the total density:

$$n(\varphi) = n_L(\varphi) + n_D(\varphi)$$

$$n(\varphi) = \int_{|\omega-\Omega|\leq KR} p_L(\varphi|\omega, t) g(\omega) d\omega + \int_{|\omega-\Omega|>KR} p_D(\varphi|\omega, t) g(\omega) d\omega \tag{1.7}$$

The conditional probability for the phase-locked group can then be obtained by solving the equation of motion (1.5), and for the drifting group it can be derived by the self-consistency assumption that it must be a stationary distribution in order to have a time-independent order parameter.

1.4 Phase distribution of phase-locked oscillators

For the phase locked group we know that for $t \to \infty$, $\dot{\varphi} = 0$ for some value of $\varphi^\star$ and ω. Thus, we solve equation (1.6) to obtain:

$$\varphi^\star = \arcsin\left(\frac{\omega - \Omega}{KR}\right), \quad \varphi^\star \in \left[-\frac{\pi}{2}, \frac{\pi}{2}\right]$$

Therefore, the conditional distribution of φ given ω is a Dirac delta function centered around $\varphi^\star$, since this is an attractor for all oscillators with natural frequency ω.

$$p_L(\varphi|\omega) = \delta\left[\varphi - \arcsin\left(\frac{\omega - \Omega}{KR}\right)\right], \quad \varphi \in \left[-\frac{\pi}{2}, \frac{\pi}{2}\right] \tag{1.8}$$

We now perform the left integral in equation (1.7) to find the density of phase locked oscillators to obtain:

$$n_L(\varphi) = \int_{\Omega-KR}^{\Omega+KR} \delta\left[\varphi - \varphi^\star\right] g(\omega) d\omega$$

but $\omega = \Omega + KR\sin\varphi^\star$ and $d\omega = KR\cos\varphi^\star d\varphi^\star$ and thus

$$n_L(\varphi) = \int_{-\frac{\pi}{2}}^{\frac{\pi}{2}} \delta\left[\varphi - \varphi^\star\right] g(\Omega + KR\sin\varphi^\star) KR\cos\varphi^\star d\varphi^\star$$

$$n_L(\varphi) = \begin{cases} g(\Omega + KR\sin\varphi)KR\cos\varphi & |\varphi| \leq \frac{\pi}{2} \\ 0 & |\varphi| > \frac{\pi}{2} \end{cases} \tag{1.9}$$

Equation (1.9) shows us that the phase locked oscillators are distributed in the half-moon around the order parameter, in accord with direct simulations of the equations of motion. Since the φ values are phase-locked, the probability distribution of synchronized oscillators n_L is also time independent, in addition to n.

1.5 Phase distribution of drifting oscillators

In order to derive the distribution of phases for drifting oscillators, for which $|\omega - \Omega| > KR$, consider an interval $[\varphi, \varphi + \delta\varphi]$ in phase values. The fraction of oscillators with natural frequency $\omega \in [\omega', \omega' + \delta\omega]$ inside this interval is given by:

$$\left[\int_{\varphi}^{\varphi+\delta\varphi} p(\varphi'|\omega)d\varphi'\right]\delta\omega \tag{1.10}$$

The change per unit time in the fraction of oscillators inside this interval is then given by the time derivative of (1.10), but since all intervals endpoints ω, $\delta\omega$ and φ, $\delta\varphi$ are fixed we have:

$$\partial_t\left[\int_{\varphi}^{\varphi+\delta\varphi} p(\varphi'|\omega)d\varphi'\right] = \int_{\varphi}^{\varphi+\delta\varphi} \partial_t p(\varphi'|\omega)d\varphi' \tag{1.11}$$

Conservation of probability inside the interval $[\varphi, \varphi + \delta\varphi]$ mandates the net change in probability is equal to the difference between fluxes at the endpoints. The probability current is written as $j(\varphi, \omega, t) = p(\varphi|\omega)\dot{\varphi}$ and therefore

$$\int_{\varphi}^{\varphi+\delta\varphi} \partial_t p(\varphi'|\omega)d\varphi' = p(\varphi + \delta\varphi|\omega)\dot{\varphi}(\varphi + \delta\varphi) - p(\varphi|\omega)\dot{\varphi}(\varphi) \tag{1.12}$$

which can be written

$$\int_{\varphi}^{\varphi+\delta\varphi} \partial_t p(\varphi'|\omega)d\varphi' = -\int_{\varphi}^{\varphi+\delta\varphi} \frac{\partial}{\partial\varphi}\left[p(\varphi|\omega)\dot{\varphi}(\varphi)\right]|_{\varphi'}d\varphi' \tag{1.13}$$

Since this equality holds for all intervals $[\varphi, \varphi + \delta\varphi]$, equating the integrands gives:

$$\partial_t p(\varphi'|\omega) + \partial_\varphi \left[p(\varphi|\omega)\dot{\varphi}(\varphi)\right] = 0 \tag{1.14}$$

We have seen that requiring the total phase distribution $n(\varphi)$ to be stationary implies that the distribution of phase-locked oscillators $n_L(\varphi)$ is also stationary. But since the distribution of drifting oscillators is given by $n_D(\varphi) = n(\varphi) - n_L(\varphi)$, it must also be stationary. Therefore $\partial_t[n_D(\varphi)] = 0$ which implies that

$$\int_{|\omega-\Omega|>KR} \partial_t[p_D(\varphi|\omega)]g(\omega)d\omega = 0 \tag{1.15}$$

Even though some time-dependent forms for $p_D(\varphi|\omega)$ might satisfy (1.15), the assumption that it is indeed stationary ties up with the original assumption about the total density n and the self consistency argument, a central point in Kuramoto's original analysis. The condition $\partial_t[p_D(\varphi|\omega)] = 0$ for all φ, together with the continuity equation (1.14) allows us to integrate $\partial_\varphi[p_D(\varphi|\omega)\dot{\varphi}(\varphi)]$ to give:

$$p_D(\varphi|\omega)\dot{\varphi}(\varphi) = C(\omega)$$

which by (1.5) results in

$$p_D(\varphi|\omega) = \frac{C(\omega)}{(\omega - \Omega) - KR\sin\varphi} \tag{1.16}$$

In order to obtain the total density $n_D(\varphi)$ we must integrate the joint distribution $p_D(\omega|\omega)g(\omega)$ over ω. In order to do that, we need to find $C(\omega)$, which can be done by using the normalization condition $\int_{-\pi}^{\pi} p_D(\varphi|\omega)d\varphi = 1$, which leads us to:

$$\frac{1}{C(\omega)} = \int_{-\pi}^{\pi} \frac{1}{\omega - \Omega - KR\sin\varphi} d\varphi \tag{1.17}$$

Using equation (2.551-3) from the integrals table [3] with the condition $|\omega - \Omega| > KR$ we get the solution:

let

$$a = (\omega - \Omega), \qquad b = KR \qquad \text{and} \qquad f(\varphi) = \arctan\frac{a\tan\frac{\varphi}{2} + b}{\sqrt{a^2 - b^2}}$$

then

$$\int \frac{1}{\pm a - b\sin\varphi} d\varphi = \pm\frac{2}{\sqrt{a^2 - b^2}} f(\varphi) \qquad a^2 > b^2 \tag{1.18}$$

which is positive for $\omega > \Omega + KR$ and negative for $\omega < \Omega - KR$. Substituting back into equation (1.17) to obtain C gives:

$$C(\omega) = \begin{cases} -\frac{\sqrt{(\omega-\Omega)^2-(KR)^2}}{2\pi} & \omega < \Omega - KR \\ \frac{\sqrt{(\omega-\Omega)^2-(KR)^2}}{2\pi} & \omega > \Omega + KR \end{cases} \tag{1.19}$$

Now, we use the expression for $C(\omega)$ to perform the integration in ω as defined in equation (1.7):

$$n_D(\varphi) = \int_{-\infty}^{\Omega-KR} \frac{C(\omega)}{(\omega-\Omega) - KR\sin\varphi} g(\omega)d\omega + \int_{\Omega+KR}^{\infty} \frac{C(\omega)}{(\omega-\Omega) - KR\sin\varphi} g(\omega)d\omega \tag{1.20}$$

To perform this integration we make use of the assumptions that g is symmetric and unimodal. In addition, we also assume that the frequency of global oscillations to which the system converges to, Ω, is coincident with the point of symmetry of g, or $\Omega = \bar{\omega}$. With this assumption, $g(\Omega + x) = g(\Omega - x)$ implying that $g(\omega)$ is identical in both integrals of (1.20) and finally:

$$n_D(\varphi) = \frac{1}{\pi} \int_{KR}^{\infty} \frac{x\sqrt{x^2 - (KR)^2}}{x^2 - (KR\sin\varphi)^2} g(x + \Omega)dx \tag{1.21}$$

1.6 Order Parameter

In the rotating frame, the Kuramoto order parameter is given by the integral:

$$R = \int_{-\pi}^{\pi} e^{i\varphi} n_L(\varphi)d\varphi + \int_{-\pi}^{\pi} e^{i\varphi} n_D(\varphi)d\varphi \tag{1.22}$$

From equation (1.21) we see that $n_D(\varphi - \pi) = n_D(\varphi)$, but $e^{i(\varphi-\pi)} = -e^{i\varphi}$, and thus the second integral is zero. The first integral on the right hand side (RHS) can then be written using equation (1.9) for the phase-locked oscillators.

$$R = KR \int_{-\pi/2}^{\pi/2} (\cos\varphi + i\sin\varphi)\cos\varphi g(\Omega + KR\sin\varphi)d\varphi \tag{1.23}$$

but since g is symmetric around Ω we end up with

$$R = KR \int_{-\pi/2}^{\pi/2} g(\Omega + KR\sin\varphi)\cos^2\varphi d\varphi \tag{1.24}$$

Thus, we see that for a fixed value of the coupling strength K there is always at least one solution for the order parameter R. The trivial (disordered) solution is given by $R = 0$. If R is non-zero, then we can divide equation (1.24) by R to obtain the condition for the existence of the solution for that particular K:

$$K \int_{-\pi/2}^{\pi/2} g(\Omega + KR\sin\varphi)\cos^2\varphi d\varphi = 1. \tag{1.25}$$

The simpler case of identical oscillators can be obtained from equation (1.25) by setting $g(x) = \delta(x - \Omega)$ which results in $K_c = 1$ as the critical coupling strength for such a network to attain synchronization.

For a general form of the natural frequency distribution g we can obtain the critical coupling strength K_c by expanding its Taylor series around Ω and neglecting terms $\mathcal{O}(R)$ and higher. This is because when $K \to K_c^+$, $R \to 0^+$ and so:

$$\frac{1}{K} = \int_{-\pi/2}^{\pi/2} \left[g(\Omega) + g''(\Omega)\frac{(KR\sin\varphi)^2}{2} + \mathcal{O}(R^3) \right] \cos^2\varphi d\varphi,$$

which gives the limit

$$\frac{1}{K_c} = \lim_{R\to 0^+} \int_{-\pi/2}^{\pi/2} \left[g(\Omega) + g''(\Omega)\frac{(KR\sin\varphi)^2}{2} + \mathcal{O}(R^3) \right] \cos^2\varphi d\varphi$$

where $g'(\Omega) = 0$ since $g(\Omega)$ is a maximum. Therefore the critical coupling is given by:

$$K_c = \frac{2}{\pi g(\Omega)} \tag{1.26}$$

As the coupling approaches the critical value from above, the order parameter scales as:

$$\frac{1}{K} = \frac{1}{K_c} - \frac{K_c^2 R^2 |g''(\Omega)|}{16} + \cancelto{0}{\mathcal{O}(R^3)}$$

which rearranged leads to

$$R(K) = \frac{4}{\sqrt{\pi K_c^3 |g''(\Omega)|}} \sqrt{\frac{K - K_c}{K_c}} \tag{1.27}$$

We see that the order parameter is sensitive to the curvature of g at its maximum, growing ever more rapidly as g becomes narrower. In the limit of identical oscillators the

order parameter becomes discontinuous at the transition. In terms of the reduced coupling strength $\kappa \equiv \frac{K-K_c}{K_c}$, the critical exponent $\beta \equiv \lim_{\kappa\to 0} \frac{\ln R(\kappa)}{\ln \kappa}$ is found to be $\beta = 1/2$, in accordance with a mean-field description or all-to-all coupling.

2 Stochastic discrete phase model

This chapter is a reproduction of the published result [4] for the first part of the thesis. Here we define the discrete three state model for coupled oscillators and investigate its behavior in circular ring graphs and give some preliminary results from simulations in small-world networks.

2.1 Summary

A lattice of three-state stochastic phase-coupled oscillators exhibits a phase transition at a critical value of the coupling parameter a, leading to stable global *oscillations* (GO). On a complete graph, upon further increase in a, the model exhibits an *infinite-period* (IP) phase transition, at which collective oscillations cease and discrete rotational (C_3) symmetry is broken. The IP phase does not exist on finite-dimensional lattices. In the case of large negative values of the coupling no synchronization is expected, but nonetheless it was shown that travelling-wave steady states are stable, displaying local order. Here, we verify the IP phase in systems with long-range coupling but of lower connectivity than a complete graph and show that even for large *positive* coupling, the system sometimes fails to reach global order. The ensuing travelling-wave state appears to be a metastable configuration whose birth and decay (into the previously described phases) are associated with the initial conditions and fluctuations.

2.2 Introduction

Systems of coupled oscillators exhibit diverse symmetry-breaking transitions to a globally synchronized state. In the paradigmatic Kuramoto model, for instance, oscillators with distinct intrinsic frequencies ω_i coupled via their continuous phases θ_i can exhibit stable collective oscillations, breaking time-translation invariance [5–9]. Amongst discrete-phase models, the paper-scissors-stone game is an example of a system with three absorbing states that can exhibit either global oscillations or spontaneous breaking of discrete rotational (C_3) symmetry [10–14]. More recently, Wood and coworkers proposed a family of models of phase-coupled three-state stochastic oscillators that undergo a phase transition to a state exhibiting global oscillations (GO) [1, 15–17] for sufficiently strong coupling. We shall refer to these as Wood's cyclic model (WCM). Although the WCM also has C_3 symmetry, it has no absorbing state. In addition to their intrinsic interest in the context of non equilibrium phase transitions, this family of models serve as a highly simplified description of collective neuronal behavior.

The first WCM [1] was found to undergo a second phase transition upon further increase of the coupling [18], at which the period of oscillation becomes infinite, thereby breaking C_3 symmetry. In [18], this infinite-period (IP) transition was studied on a complete graph (all-to-all coupling), and a novel order parameter, involving the mean rate of change of the probability distribution, was proposed. On the basis of a nucleation scenario, the authors of Ref. [18] argued *against* the existence of an IP transition on finite-dimensional lattices with short-range interactions, but left open the question of its occurrence on networks with nonlocal interactions. Here we study a WCM on (1) regular rings with interactions up to $2K$-neighbors, varying the interaction range K, and (2) small-world networks. Using numerical simulations to study the order parameter and its variance, we verify the existence of GO and IP phase transitions on these structures. For regular rings of N nodes, the degree of connectivity is characterized by $\alpha \equiv K/N$ such that $\alpha \in (0, 0.5)$. A key question is the minimum value of α necessary to observe the GO and IP phases as $N \to \infty$. Our results suggest that any $\alpha > 0$ is sufficient.

We also provide evidence that for intermediate interaction ranges, global synchronization depends sensitively on initial conditions: Some realizations with a random initial configuration show no global synchronization. Such events persist even as the number of neighbors grows in proportion to the system size. In this situation, the final state may be a travelling wave, as observed by Escaff et al. [19] in the case of *anti-crowding*, i.e., interactions favoring anti-synchronization between neighbors.

The remainder of this paper is organized as follows. In section 2.3 we review the WCM and the essentials of the transitions to the GO and IP phases. We report our results on the GO and IP phase transitions on regular rings, and on small-world networks, in sections 2.4 and 2.5, respectively. Our conclusions are discussed in section 2.6.

2.3 Model

In the WCM, the state s^x at site x ($x = 1, \ldots, N$) can take one of three values, $s^x \in \{0, 1, 2\}$, corresponding to a phase $\phi^x = 2\pi s_x/3$. The only allowed transitions are

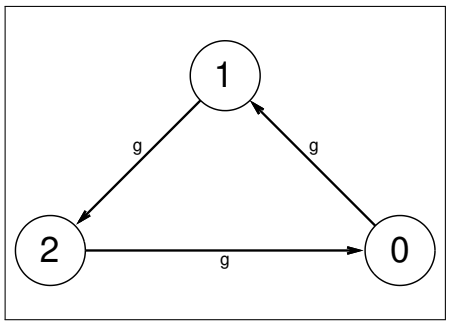

Figure 1 – Transition rates for an isolated unit.

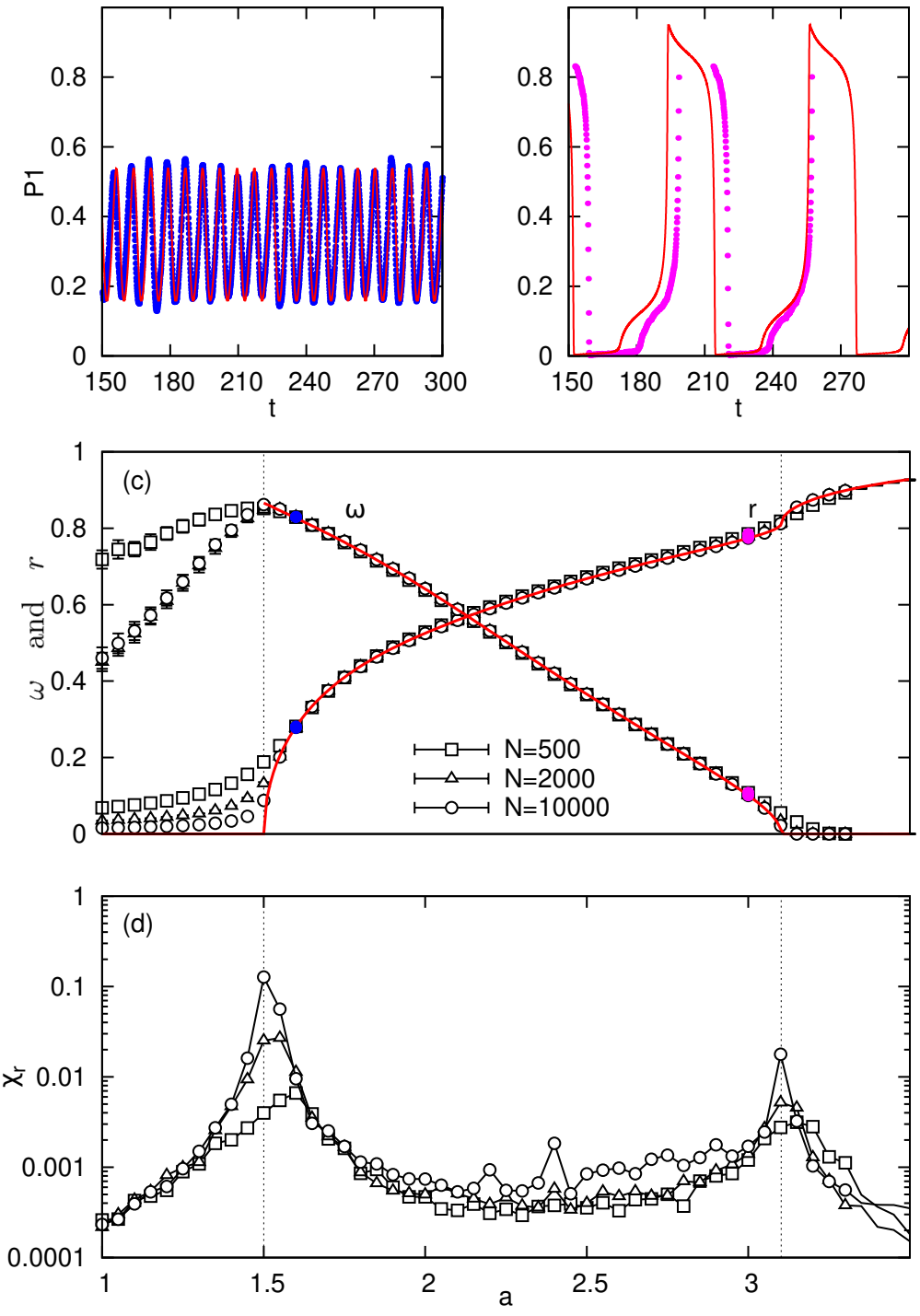

Figure 2 – (Color online) Panels (a) and (b) show the evolution of P_1 for $a = 1.6$ and $a = 3$, respectively. Points: simulations of a complete graph of N nodes; lines: MF solution. (c) Dependence of r and ω on a, exhibiting the two phase transitions. (d) χ_r versus a, showing peaks at the transitions [system sizes as in (c)].

those from s to $s+1$ (modulo 3) (see Fig. 1), which implies that detailed balance is violated. If site x is in state $s^x = j$, its transition rate to state $j+1$ is:

$$\gamma_j^x = g \exp\left[a \frac{\left(n_{j+1}^x - n_j^x\right)}{n^x}\right] \tag{2.1}$$

where g is a constant, a is the coupling parameter, n_j^x is the number of neighbors of site x in state j, and n^x is the number of neighbors for site x. Since these rates are invariant under cyclic permutation of the state indices, the model is invariant under the group C_3 of discrete rotations.

Let N_j be the total number of sites in state j, so that $N_0 + N_1 + N_2 = N$, the total number of sites. As discussed in [18], the MF approximation, obtained by replacing n_j^x/n^x in the argument of the exponential of Eq.(2.1) with the corresponding state fraction, $n_j = N_j/N$, yields three non equilibrium phases, separated by two continuous phase transitions. For small coupling ($a < a_c = 1.5$), the disordered phase, with $\mathbf{n} = (1/3, 1/3, 1/3) \equiv \mathbf{n}_{1/3}$, is the stable stationary solution of the MF equations. ($\mathbf{n}$ denotes the vector of state fractions.) For a between a_c and a higher value, $a^c \simeq 3.102\,439\,915\,64$, there is no stable stationary solution and the MF equations admit an oscillatory solution (a limit cycle) in which states 0, 1 and 2 periodically assume the role of the majority. As a is increased above a_c, the frequency ω of oscillation decreases continuously, becoming zero at a^c, signalling the IP transition. For $a > a^c$, three stationary solutions, $\mathbf{n}_j$ appear, such that state j represents the (permanent) majority. Thus C_3 symmetry is broken for $a > a^c$. (The three solutions are, naturally, related via cyclic permutation of indices in state space.)

The WCM is characterized by a pair of order parameters. First, one has the familiar Kuramoto synchronization parameter [1, 5, 7],

$$r \equiv \langle \langle |v| \rangle_t \rangle_s \,, \tag{2.2}$$

where

$$v \equiv \frac{1}{N} \sum_{x=1}^{N} e^{i\phi^x} . \tag{2.3}$$

In Eq. (2.2), $\langle\rangle_t$ denotes a time average over a single realization (in the stationary state), and $\langle\rangle_s$ an average over independent realizations. Note that $r > 0$ is consistent with, but does not necessarily imply, globally synchronized oscillation. The latter is characterized by a periodically varying phase of v [20–23].

In the MF analysis, the transition to the synchronized regime (the GO transition) is associated with a supercritical Hopf bifurcation at $a = a_c = 1.5$: the trivial fixed point $\mathbf{n}_{1/3}$ loses stability at $a = a_c$, and a limit cycle encircling this point appears. For $a \gtrsim a_c$, sustained oscillations in n_j characterize synchronization among the oscillators (Fig. 2a).

Correspondingly, r grows continuously $\sim (a - a_c)^\beta$ at the transition (Fig. 2c), with a MF exponent $\beta = 1/2$ [1]. The scaled variance

$$\chi_r \equiv L^d \left[\left\langle \langle |v| \rangle_t^2 \right\rangle_s - r^2 \right], \tag{2.4}$$

diverges with the system size at criticality, as shown in Fig. 2d for simulations on the complete graph [18]. The GO transition is associated with breaking of the continuous time-translation symmetry: the $\mathbf{n}_k(t)$, are periodic for $a \gtrsim a_c$. Increasing a above a_c enhances synchronization among the oscillators, leading to increasing oscillation amplitudes, as shown in Fig. 2b.

Wood *et al.* found that the increasing amplitude of oscillation is accompanied by a decreasing angular frequency $\omega = 2\pi/\langle\tau\rangle$, where $\langle\tau\rangle$ is the mean time between peaks in n_k (Figs. 2a-c). This can be understood qualitatively from the exponential dependence of the transition rates of Eq. (2.1) on the neighbor fractions: When a state is highly populated, the rate at which oscillators leave it becomes very small. In the MF theory, when a reaches the upper critical value a^c, three symmetric saddle-node bifurcations occur simultaneously, and the period of the collective oscillations diverges [18]. Above a^c, there are three symmetric attractors in the system, and 3-fold rotational (C_3) symmetry is spontaneously broken. As in condensation or a ferromagnetic phase transition [24], freezing of the majority state does not imply that individual oscillators freeze as well. The transition rates of individual oscillators do decrease with increasing a, but only vanish in the limit $a \to \infty$, when one of the states is fully occupied.

It is convenient to define an order parameter ψ that is identically zero (in the infinite-size limit) for $a > a^c$. Assis et al. proposed [18],

$$|\psi| \equiv \frac{1}{N} \left| \sum_{x=1}^{N} \left(\delta_{0,s^x} + e^{2\pi i/3} \delta_{1,s^x} + e^{-2\pi i/3} \delta_{2,s^x} \right) \gamma^x \right| \tag{2.5}$$

where δ_{ij} is the Kronecker delta and $\gamma^x \equiv \gamma^x_{s^x}$ is the transition rate at site x (see eq. 2.1). Thus $|\psi|$ involves not only the configuration, but the rate at which the latter evolves. On the complete graph, γ^x is the same for all sites x in the same state j. Denoting this rate by γ_j, the order parameter can be written (in MF analysis) as

$$|\psi|^2 \overset{MF}{=} \sum_{j=0}^{2} (n_j \gamma_j - n_{j-1} \gamma_{j-1})^2 \tag{2.6}$$

Both the disordered phase ($a < a_c$) as well as the IP phase ($a > a^c$) have stable, stationary solutions, $\mathbf{n}^*$. Since $\dot{n}_j = 0$ implies $n^*_j \gamma_j = n^*_{j-1} \gamma_{j-1}$, i.e., zero net change in the probability

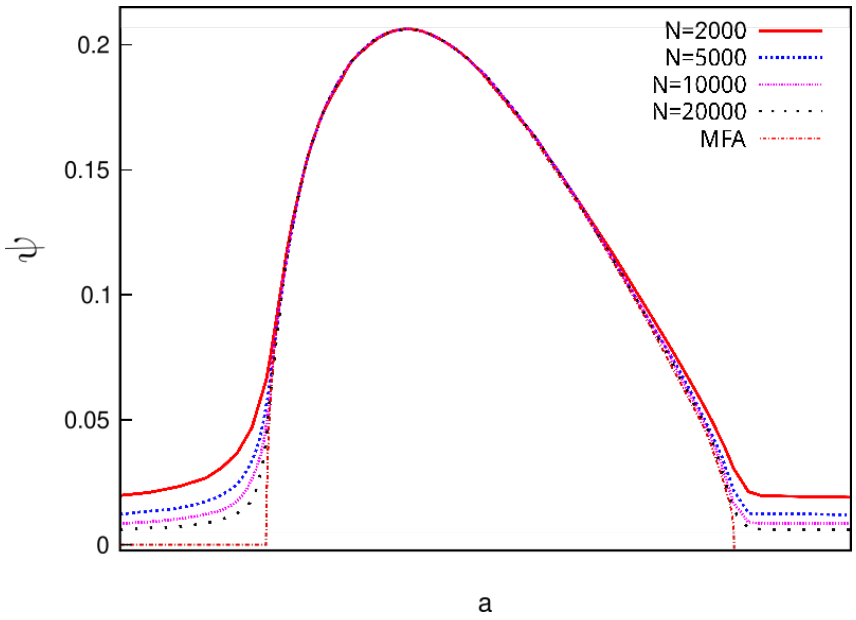

Figure 3 – (Color online) (From [18].) Order parameter $\langle|\psi|\rangle$ as a function of coupling a in the MF theory and on the complete graph, for sizes as indicated.

of state j, we have $|\psi| = 0$ in eq. 2.6 for both cases [a similar line of reasoning can be applied directly to Eq. (2.5)].

Figure 3 shows $\langle|\psi|\rangle$ versus a in MF theory, and on the complete graph (the latter via numerically exact solution of the master equation), confirming that $|\psi|$ functions as an order parameter to detect both the GO and IP phase transitions. The MF critical behavior is $\langle|\psi|\rangle \sim (a - a_c)^{1/2}$ for $a \searrow a_c$ and $\langle|\psi|\rangle \sim (a^c - a)^{1/2}$ for $a \nearrow a^c$. On the complete graph, the order parameter decays with system size as $\langle|\psi|\rangle \sim N^{-1/4}$ at $a = a_c$ and as $N^{-0.4203(3)}$ at $a = a^c$. The first result is typical of MF scaling with system size at a continuous phase transition, as argued in [18].

The results for the IP transition in MF and on a complete graph are in sharp contrast to what is found on finite-dimensional lattices. The *absence* of such a transition was verified numerically on hyper cubic lattices in dimensions $d \leq 4$ in [18]. This reference also provides a quantitative argument showing that on finite-dimensional lattices, a j-state majority cannot persist indefinitely: it is always susceptible to change via nucleation of a cluster of state $j + 1$. The authors of [18] conjectured that the IP transition would occur on structures in which a site interacts with a nonzero fraction of all other sites (as the system size tends to infinity). In the following sections we test this conjecture on two structures, regular rings with extended interactions, and small-world networks.

2.4 The WCM on regular rings

A *regular ring* is constructed starting from a graph of N nodes arranged in circular fashion. Considering one node at a time in a clockwise manner, we connect it to its K nearest neighbors in the clockwise direction; an example of such a structure is shown in Fig. 4. We define the *connectivity* of a regular ring graph by $\alpha \equiv K/N$, such that $\alpha = 1/N$ signifies a one-dimensional chain while $\alpha = 0.5$ represents a complete graph. Thus, one can interpolate from the one-dimensional to an infinite-dimensional hyper cubic lattice (complete graph) varying α over the interval $\left(0, \frac{1}{2}\right]$. It is known that the WCM on hyper cubic lattices of dimensions 1 and 2 cannot sustain ordered phases [1, 18]. Since $\alpha = 0.5$ represents the complete graph, there must be at least one threshold $\alpha = \alpha^*$ above which one or both phase transitions (GO and IP) occur, varying a.

Different from hyper cubic lattices, in which coupling is local, for $\alpha > 0$ the coupling on ring graphs is nonlocal. The manner in which the interaction range scales as $N \to \infty$ can be chosen in different ways; the simplest, which we consider here, is to fix α so that $K \propto N$ (More precisely, $K = \lceil \alpha N \rceil$ where $\lceil x \rceil$ denotes the smallest integer larger than x). It is reasonable to expect that phase transitions occur for any fixed $\alpha > 0$, since the interaction range K then tends to infinity with N.

2.4.1 Scaling behavior: phase boundary

The dynamics as N increases can be studied by defining the scaled variances of the order parameters. These quantities are expected to diverge in the thermodynamic limit when the system undergoes a continuous phase transition [25]. The scaled variances of

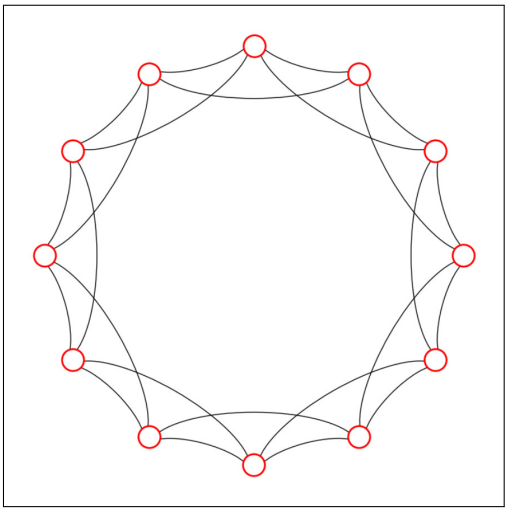

Figure 4 – A regular ring is an undirected graph with N nodes arranged in circular fashion, with each connected to its K nearest neighbors in each direction. Here we show an example with $N = 12$ and $K = 2$.

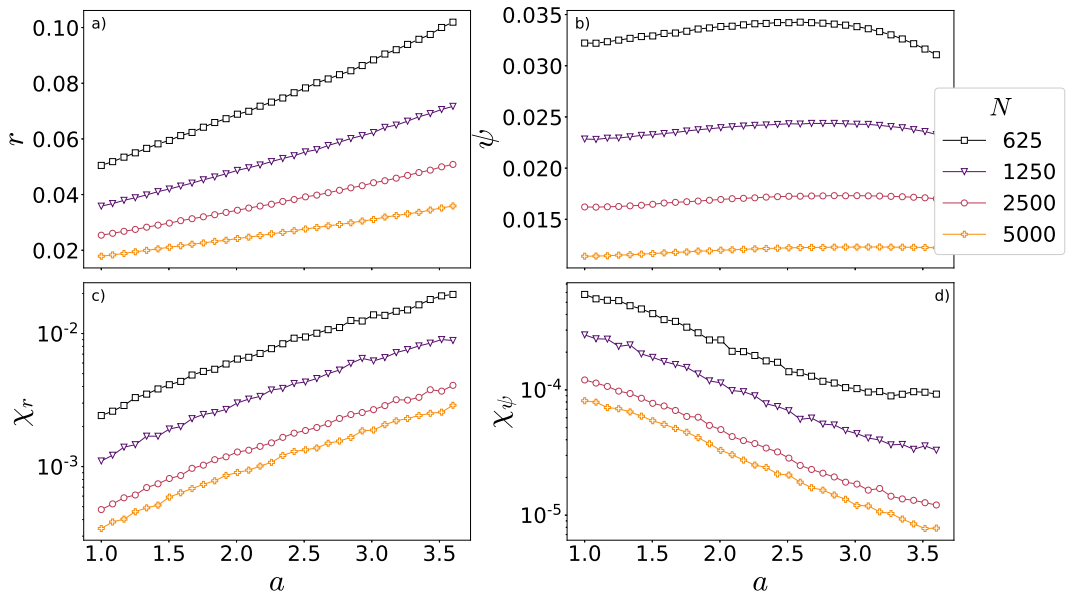

Figure 5 – (Color online) Order parameters and their scaled variances for one-dimensional rings ($K = 1$). Both the order parameters and their respective variances decrease as the system size is increased, with $r \approx \psi \approx 0$ across a wide range of coupling strengths. Points represent an average over 3000 independent realizations with random initial configurations. For the 1D chain, the same behavior is observed regardless of initial configuration.

order parameters r and ψ can be defined through equations 2.3 and 2.5 as:

$$\begin{aligned} \chi_r &= N\left[\left\langle \langle |v| \rangle_t^2 \right\rangle_s - \langle \langle |v| \rangle_t \rangle_s^2\right], \\ \chi_\psi &= N\left[\left\langle \langle |\psi| \rangle_t^2 \right\rangle_s - \langle \langle |\psi| \rangle_t \rangle_s^2\right], \end{aligned} \tag{2.7}$$

where $\langle\rangle_t$ and $\langle\rangle_s$ are averages over time and over independent realizations, respectively.

In simulations, the system is allowed to relax to a steady state, starting from its initial configuration. Once the steady state has been attained, the order parameters are averaged over the remainder of the evolution. As we will see, the choice of initial condition is important for some values of the interaction range K; we will focus on two different setups: *random* initial configurations, in which the initial phase of each oscillator is chosen uniformly and independently among the three possible values in $\{0, 2\pi/3, 4\pi/3\}$, and a *uniform* initial condition, in which $\phi_i = 0,\ \forall i$.

In the following we describe results for uniform initial conditions. In Fig. 5 we plot the order parameters and their associated variances for $K = 1$ (i.e., $\alpha = 1/N$). Both quantities are shown to decrease with system size (for the 1D case in particular this behavior is the same regardless of initial configuration), indicating the absence of phase transitions. In Fig. 6, the same quantities are shown for regular rings with $N = 1000$ and

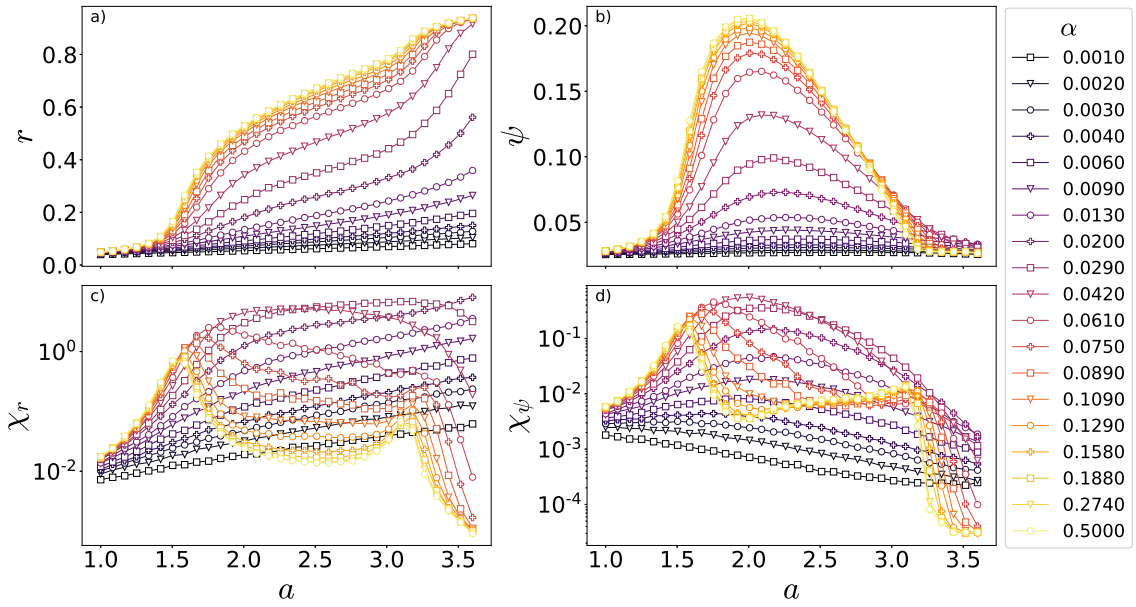

Figure 6 – (Color online) Order parameters and scaled variances for regular rings of size $N = 1000$ and various values of the connectivity α. Points represent an average over 4000 independent realizations with uniform initial configurations.

various α values. As expected, the order parameters and their variances approach the complete-graph limit as α nears the value $1/2$. Denoting by α^* the value associated with a change from one to two maxima in χ_ψ, we identify $\alpha^* \approx 0.06$ for $N = 1000$ in Fig. 6. Performing similar analyses for different system sizes we obtain α^* as a function of N. To infer the scaling behavior, we define $\lambda \equiv N^{-1}$ and look at the α^* versus $\sqrt{\lambda}$ curve near $\lambda = 0$. The resulting data, shown in Fig. 7, suggest that α^* tends to zero as $N \to \infty$. This supports the conjecture stated previously that in this limit, and for any fixed $\alpha > 0$, the WCM on a regular ring lattice exhibits both GO and IP phase transitions.

2.4.2 Scaling behavior: order parameter

To better understand the scaling behavior we look at the order parameters as $N \to \infty$ with fixed α. If both r and ψ tend to zero, there is no global synchronization. Both order parameters tending to positive values indicates the presence of global or intermittent synchronization among large populations of oscillators, while $\psi \to 0$ with $r \sim 1$ defines an infinite-period phase.

In this context it is useful to plot the order parameter versus $\lambda \equiv 1/N$. An upward (downward) curvature as $\lambda \to 0$ signals a nonzero (zero) value of the order parameter. In Fig. 8, such plots are shown for selected values of α [1] and system sizes up to $N = 10^4$. In panel b) we see evidence of the GO transition for the value $\alpha = 0.0017$ in the form of an

[1] See full animations of Fig. 8: GO transition, IP transition

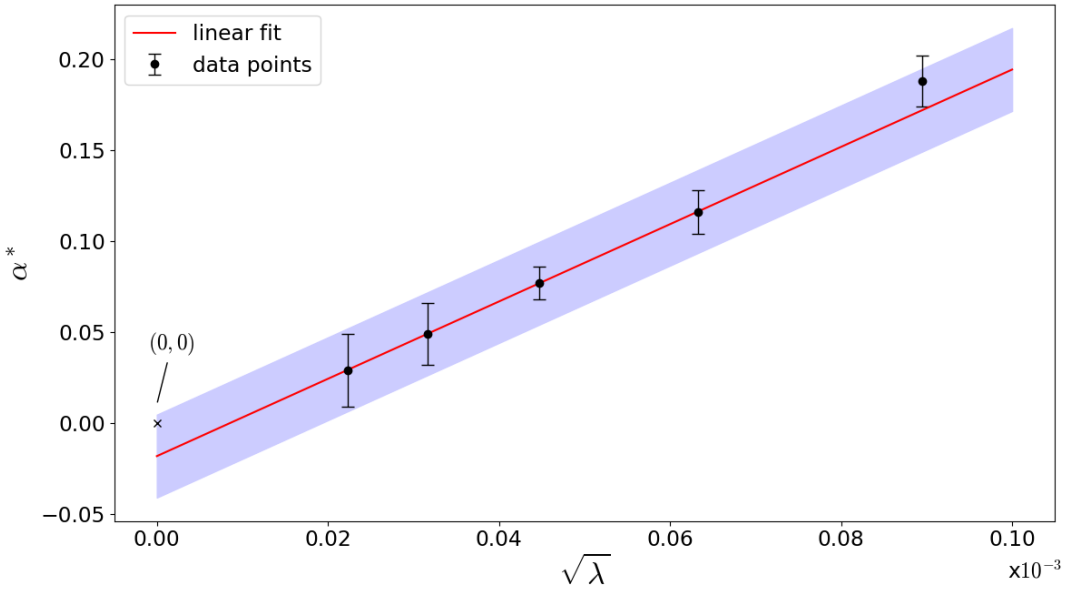

Figure 7 – Plot of α^* versus $\sqrt{\lambda}$. Starting from uniform initial configurations, $\alpha > \alpha^*$ means χ_ψ and χ_r exhibit two maxima, whereas for $\alpha < \alpha^*$ only a single broad maximum is observed. Full circles represent data obtained from simulations and solid curve is a linear fit with equation $y = -0.01837 + 2.1271x$. The band around the fitted curve represent the uncertainty associated with the linear intercept.

inversion in curvatures for lines of constant coupling strength, which happens at $a_c \approx 2$. The inset in this same panel shows that for large α there is a clear split near the complete graph value $a_c = 1.5$. In the case of the IP transition we observe that there is no upward curvature at any point, but rather a sharp increase in density of the lines of constant a for higher values of α, as seen in the bottom inset of Fig. 8 where the lines $a = 3.375$ and $a = 3.306$ have collapsed to the same point near the origin.

Inspecting individual realizations of the dynamics in the small-α regime (Fig. 9) we see that the system never shows global synchronization. It instead exhibits wave-like patterns that propagate in both directions, similar to what is observed for large negative coupling [19], but here for a positive . The amplitude and period of the wave increase with a and with system size (for fixed α), which suggests there is an IP phase in the limit $N \to \infty$.

2.4.3 Initial configuration dependence

Up to this point, all the results discussed were obtained using uniform initial configurations (ICs). In Fig. 10 shows χ_r and χ_ψ for *random* ICs. The striking difference, compared to the results for uniform ICs, is the presence of a middle peak between the two identified previously. The scaling behaviors (panels **b** and **d**) suggest that the effect

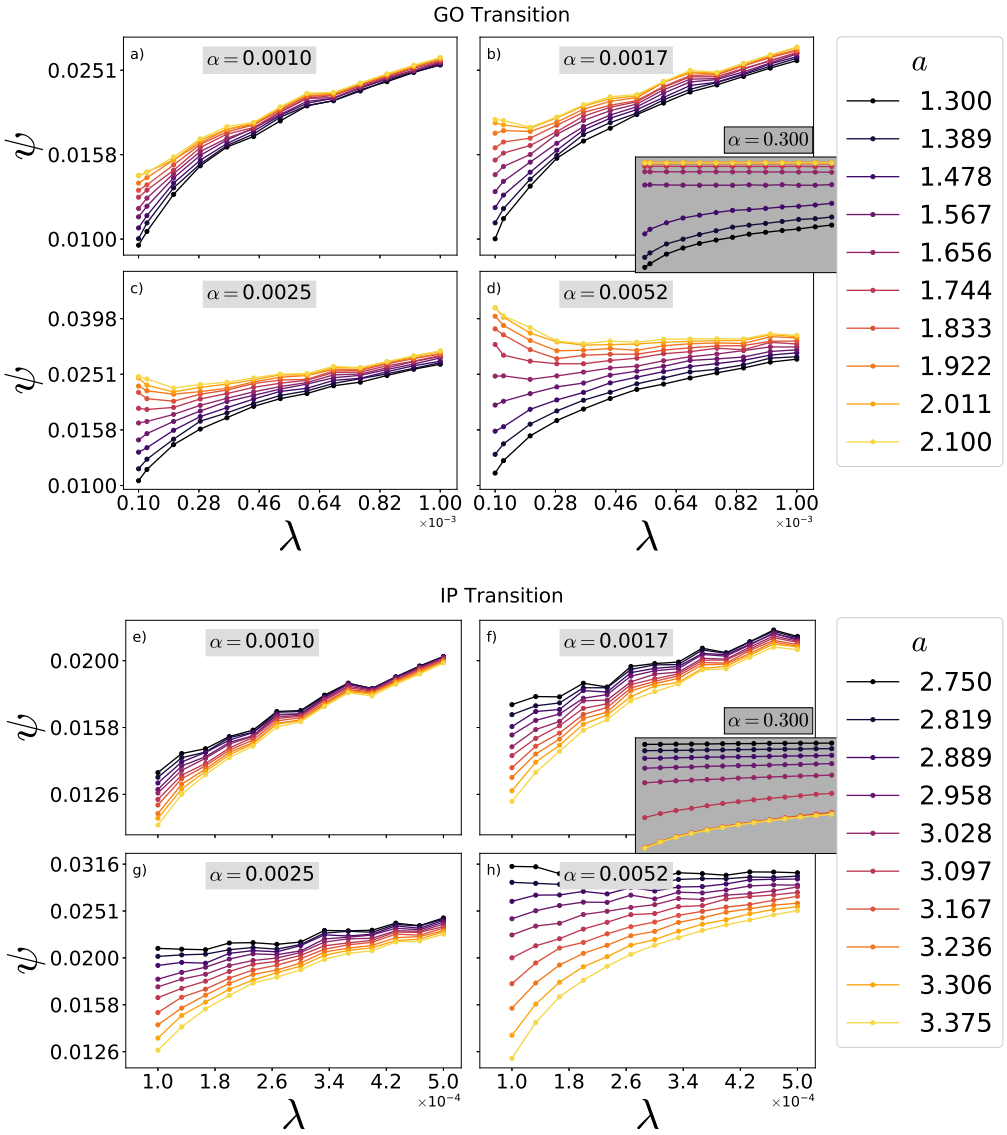

Figure 8 – (Color online) Order parameter ψ versus inverse system size λ for various values of α, and coupling strengths a in the vicinity of the GO and IP phase transitions. The insets in **b** and **f** show the behavior for $\alpha = 0.3$, approaching the complete graph, with GO and IP transitions near $a_c = 1.5$ and $a^c \approx 3.1$ respectively. Each point represents an average over 400 independent realizations. The oscillatory behavior seen in some panels is due to the reduction in average path lengths caused by the introduction of new neighbors as the system size increases at fixed α, and the fact that K must be an integer (see Appendix A).

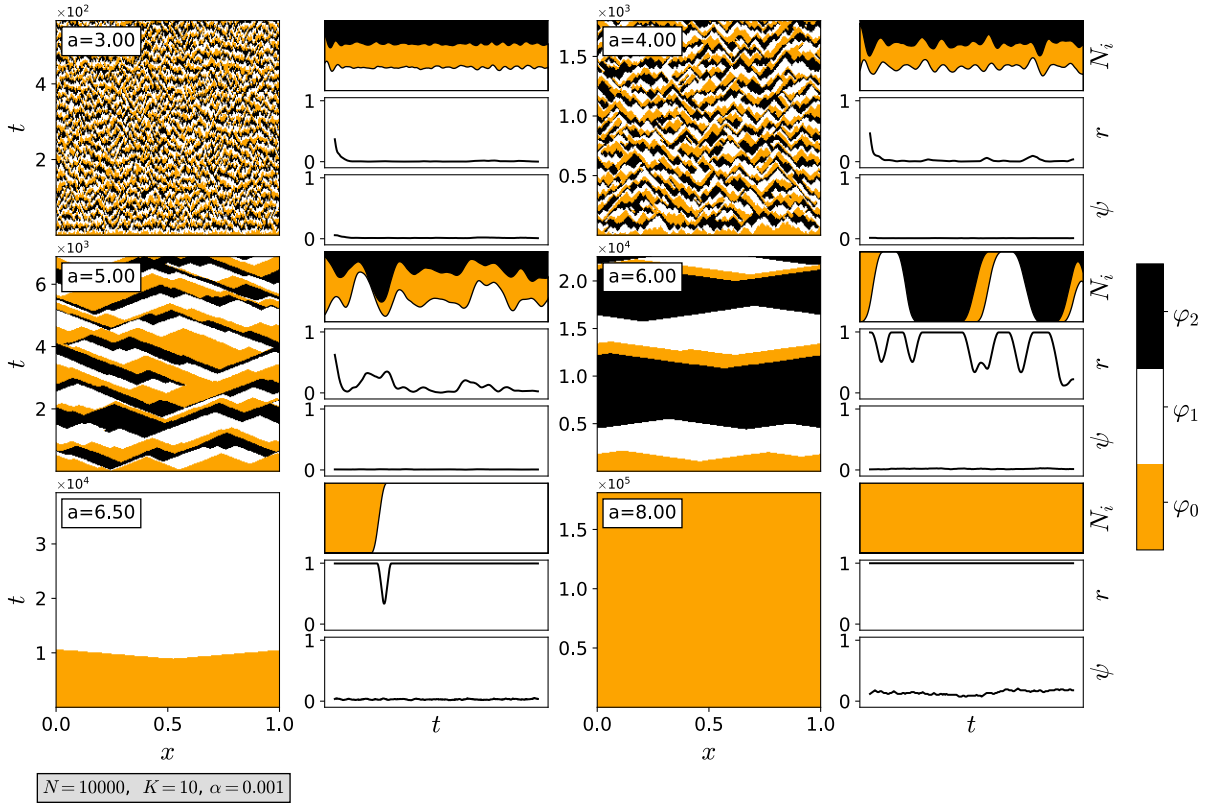

Figure 9 – Space-time plots, populations N_i, ψ and r order parameters. In all panels $N = 10^4$, $K = 10$ and $\alpha = 10^{-3}$. The images on the left and center-right columns show space-time plots with position on the horizontal axis and time increasing upward. Adjacent and to the right of each space-time plot, three graphs show the corresponding populations, ψ, and r as functions of time. Here we see that for a large system with low connectivity there are no regular oscillations. Instead, there are wave fronts that propagate and interfere and whose periods and amplitudes grow with a.

persists for large system sizes if α is held constant. High values of χ result from multiple realizations of the dynamics that produce net averages of the order parameter that differ from one to another. At the (continuous) GO and IP phase transitions, the values of the order parameter fluctuate strongly, giving rise to the peaks at $a = 1.5$ and $a \approx 3.1$. Another situation which may lead to high χ values is a bi-stability between configurations that have large values of the order parameter and others having a small one, even when fluctuations associated with each configuration are small. This suggests a *discontinuous* phase transition where for some values of α the system can relax to multiple steady states.

Space-time plots of the dynamics with coupling $a \approx 2.5$ and $\alpha = 0.14$ reveal that this is indeed the case (Fig. 11). Three examples are shown in Fig. 11: on the left is the familiar globally synchronized state, while the middle panel shows a travelling-wave state similar to those observed in [19], (but here, for large, positive coupling). The existence of a steady state with zero order parameter but $a > a_c$ is surprising since Fig. 10 suggests

that wave-like solutions persist even in the limit $N \to \infty$ (with fixed α), where interaction ranges become infinite.

The rightmost panel in Fig. 11 shows a fluctuation-induced change from a travelling wave to global synchrony. Such transitions allow the average order parameter to attain values between those associated with a wave state and a globally synchronized one, being closer to one or the other depending on what fraction of time it spent at that particular configuration. Starting from *random* ICs, about 1.6% of realizations exhibit travelling waves, but since $\psi \approx 0$ for the waves and $\psi \sim \mathcal{O}(1)$ for the globally synchronized case, the variances χ_r and χ_ψ are sensitive even to small rates of occurrence. Due to fluctuations, waves do not persist in smaller systems; sizes $N \geq 700$ are required. Smaller systems exhibit either disordered phases with domains that increase in size and duration as the coupling grows, or global synchrony if the interaction range K is large enough. In all cases, waves with exactly one spatial period over the system are observed, while for negative coupling, multiple stable wave numbers are found depending on the coupling magnitude [19].

The existence of travelling waves can be understood by noting that, for $\alpha < 0.5$, the system consists of $G = N/2K$ domains. G represents the average path length for regular rings. (See Appendix A.) When G is a multiple of three, the system is capable of containing a full wavelength without oscillators in the center of the domains. The wavefronts are then able to propagate as nucleation fronts [18] giving rise to travelling waves. In our

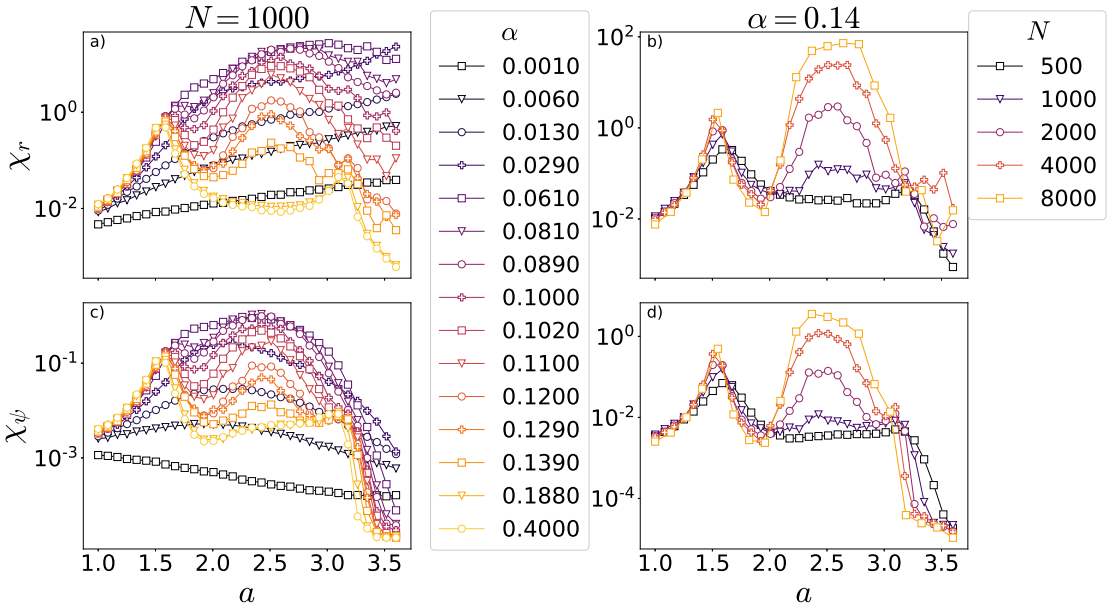

Figure 10 – (Color online) Scaled variances χ_r and χ_ψ for random initial conditions. Left column: fixed system size $N = 1000$ with increasing α. Right column: fixed $\alpha = 0.14$ and increasing system sizes. Points represent an average over 4000 independent realizations with random initial configurations.

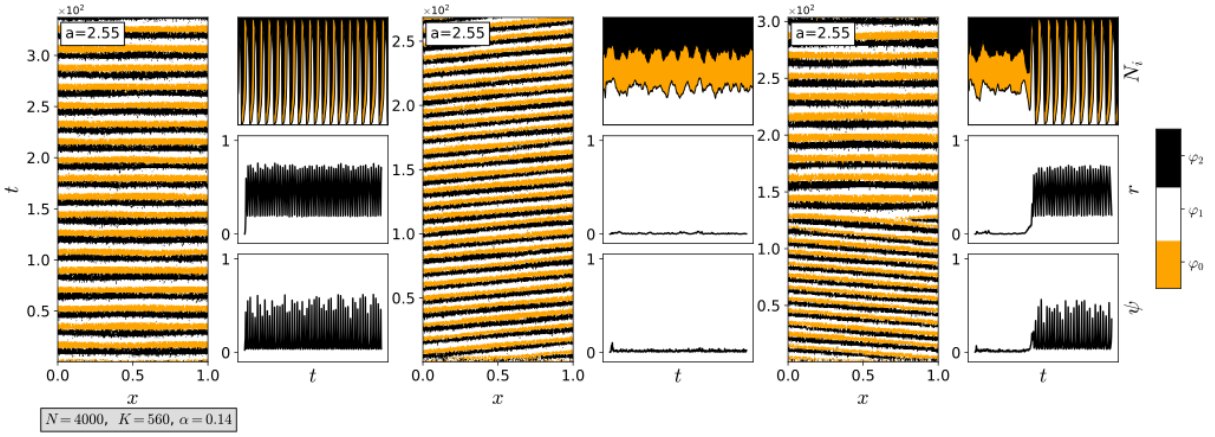

Figure 11 – Single realizations with random initial configurations. Left: Global oscillations. Middle: travelling wave. Right: fluctuation-induced change from a travelling wave to global oscillations. The fraction of realizations that converge to travelling waves is approximately 1.6%. In all panels $N = 4000$, $K = 560$, $a = 2.55$.

simulations, with $N \leq 10^4$, we find only one stable wave-number (a wave with period N). This is in contrast with the wave patterns observed in [19], where multiple wave-numbers were identified as stable depending on the magnitude of the coupling strength.

Although travelling waves are rare starting from random ICs, initializing with solid blocks of 0s, 1s and 2s, each occupying one third of the system, the ensuing evolution consists of a stable travelling wave in nearly all cases. Thus the rarity for random ICs simply reflects the low probability of provoking a wave, and does not reflect an intrinsic instability of the travelling-wave state. ICs with smaller blocks, such that the system contains two or more waves, invariably yield, following a transient, a travelling wave whose wavelength equals the system size.

With the known phase transition points for $\alpha = 0.5$ and the data from Figs. 10 and 8 (for $N \leq 10^4$) we are able to sketch the phase diagram (Fig. 12). While the phase boundaries are rather insensitive to changes in the connectivity for relatively large α values, they veer to larger couplings for small α.

2.5 The WCM on small-world networks

Regular rings can be used as the starting point for constructing *small-world networks*, which are characterized by a small degree of separation between nodes while maintaining local regions tightly clustered. A well known algorithm for generating this type of network from regular rings was introduced by Watts and Strogatz [26]. Starting from a regular ring, for each edge in the graph, the clockwise node of that edge is swapped with probability p for another randomly selected node, forbidding self-connections or repeated

edges. Some care may be taken to avoid disconnected graphs as a result of this process, but this is unlikely for most parameter triplets (N, K, p) considered here [26]. An example of such a rewired ring is shown in Fig. 13.

To characterize a network as small-world, we define two quantities:

- *Mean path length* L: For nodes i and j in network $\mathcal{G}$, let L_{ij} be the number of edges in the shortest path connecting these nodes. Then the average path length of $\mathcal{G}$ is $L = \langle L_{ij} \rangle$, where the average is over all pairs (i, j) with $i < j$.
- *Clustering coefficient* C: If node i has n_i neighbors, then the maximum possible number of connections among its neighbors is $m_i = \frac{n_i(n_i-1)}{2}$. Let m_i^* be the number of connections among the neighbors of node i in network $\mathcal{G}$. Then the clustering coefficient of $\mathcal{G}$ is $C = \left\langle \frac{m_i^*}{m_i} \right\rangle$, where the average is over all nodes i.

Evidently, the maximum possible value for C is $C = 1$ and the minimum possible value for L is $L = 1$. For networks generated by rewiring a regular ring graph, C and L are functions of the ring-graph parameters N and K, as well as the rewiring probability p: $L \equiv L(N, K, p)$, $C \equiv C(N, K, p)$. As shown in the Appendix, for regular rings (i.e., $p = 0$), we have:

$$C(N,K,0) = \begin{cases} 0, & \text{if } K < 2 \\ \frac{3K-3}{4K-2}, & \text{if } 2 \le K \le \frac{N-1}{3} \\ \frac{12K^2+6K-6KN+N^2-3N+2}{4K^2-2K}, & \text{if } \frac{N-1}{3} < K < \frac{N}{2} \\ 1, & \text{otherwise} \end{cases} \tag{2.8}$$

$$L(N,K,0) = \begin{cases} \frac{KG(G-1)+rG}{N-1}, & \text{if } K \le \frac{N}{2} \\ 1, & \text{otherwise,} \end{cases} \tag{2.9}$$

where G is the largest integer smaller than $\frac{N-1}{2K}$ or, using the floor operator,

$$G = \left\lfloor \frac{N-1}{2K} \right\rfloor.$$

For nonzero values of p we generate graphs and take the averages for C and L, as shown in Fig. 14. For rewiring probabilities $p \in (0.001, 0.1)$, rewiring preserves the clustering property while greatly reducing the average path length, thus characterizing small-world networks.

Since rewiring creates long-range interactions that reduce path lengths globally, we expect it to facilitate synchronization. This is shown to be the case in Fig. 15, where p is gradually increased: realizations starting from *random* initial conditions are shown to

readily synchronize for very small values of p, leading to the usual three phases identified for the complete graph. This means that the introduction of very few global connections is sufficient to destabilize travelling waves; they are virtually absent for $p \approx 0.01$. In Fig. 16 a histogram of the average order parameter per realization, $\langle\psi\rangle_t$, shows that the fraction of time spent in wave configurations is drastically reduced by the introduction of the rewiring procedure. When $p \geq 0.01$ and $a_c < a < a^c$, the system quickly converges to the GO phase even if it initially acquired a wave-like solution (see Fig. 17). Moreover, if system size is increased at constant α, smaller values of p are sufficient to cause the same effect, which is consistent with the fact that the number of long range connections is proportional to NK.

Following the same procedure as before, we plot in Fig. 18 the order parameters versus inverse system size λ. Here we fix α at a low value ($\alpha = 0.0052$) and vary p. [2] Comparing these results with panels d) and h) of Fig. 8 we see that the mean absolute value of ψ is much greater when p lies in the small-world region, indicating greater synchrony among oscillators. Space-time plots for values of $p > 0$ show that indeed travelling waves become unstable, so that the system exhibits only the three phases observed on the complete graph, namely, disordered, GO and IP phases. The phase diagram remains similar to the case of regular rings, displaying low sensibility to α except for very small values where the discreteness of finite systems becomes apparent. The main difference is that for any positive p wave-like steady states are absent and thus the phase diagram contains only three macroscopically distinct phases.

[2] See full animations of figure 18: GO transition, IP transition

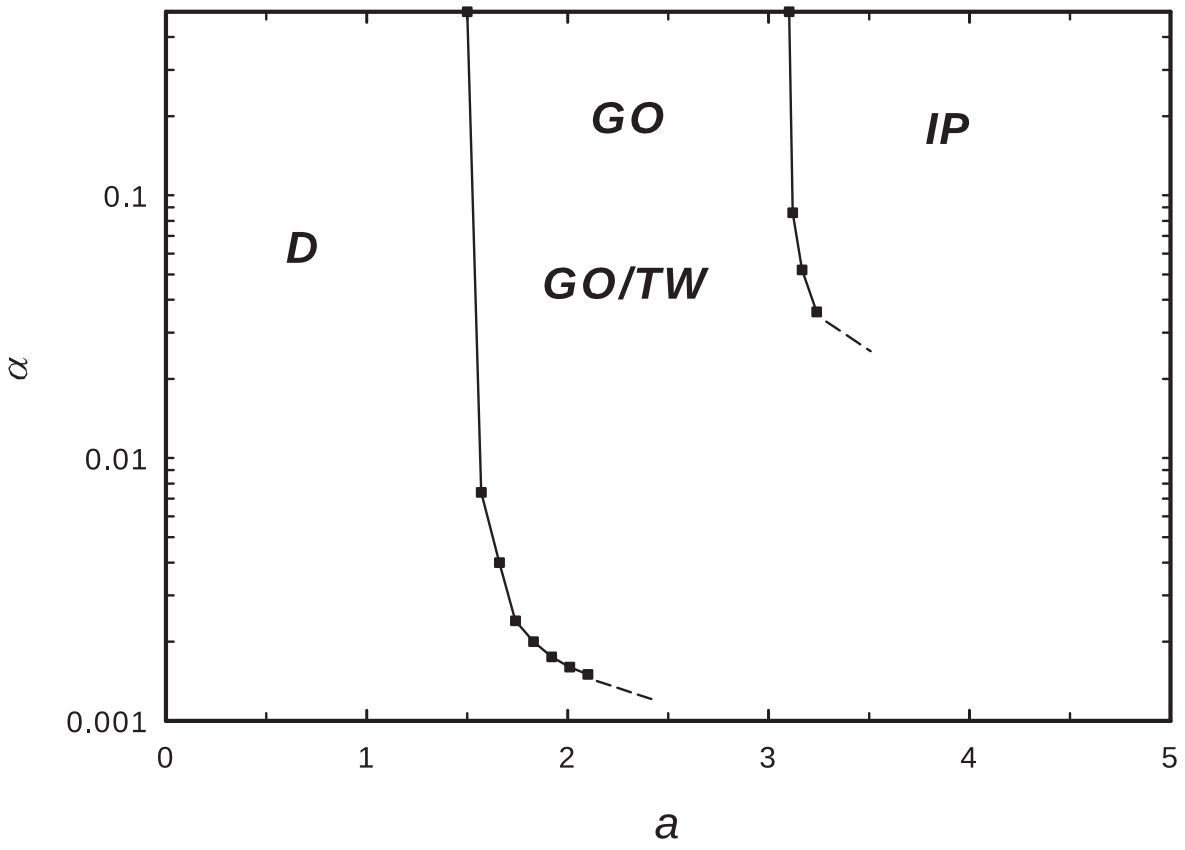

Figure 12 – Regular rings: Preliminary phase diagram in the a-α plane. Points are simulation results and (for $\alpha = 0.5$) exact values. Lines are guides to the eye. Dashed lines represent our conjectures for how the phase boundaries continue. Phases: disordered (D); global oscillation (GO); travelling-wave (TW); infinite- period (IP).

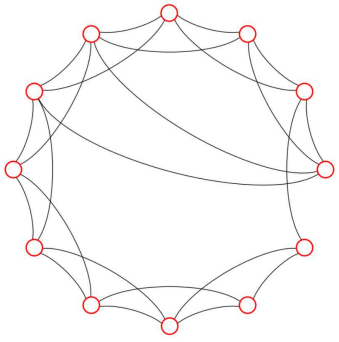

Figure 13 – Example of a rewired regular ring with $N = 12$, $K = 2$ and $p = 0.1$.

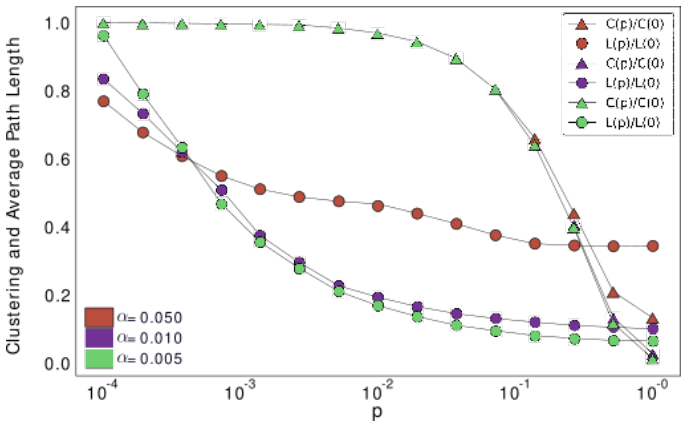

Figure 14 – (Color online) Clustering coefficient C and mean path length L versus rewiring probability p for networks of $N = 5000$ nodes. $K = 250, 50, 25$ for red, blue, green curves respectively. The data represent averages over 400 independently generated networks.

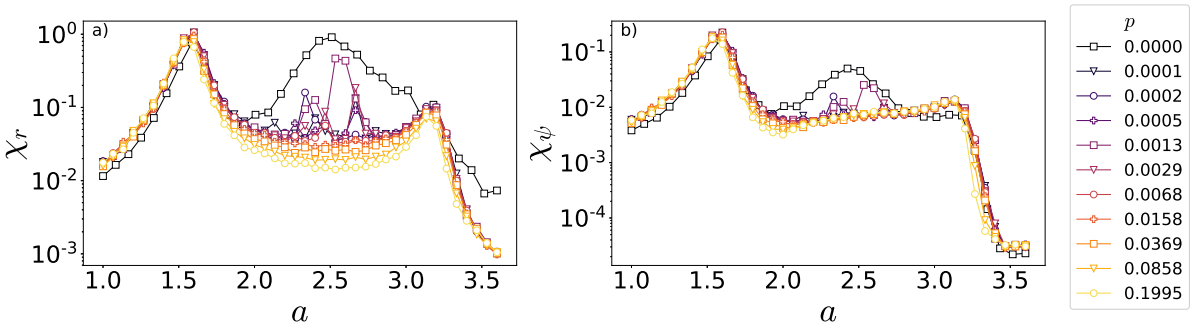

Figure 15 – (Color online) Small-world networks: Scaled variances, χ_r and χ_ψ, for increasing rewiring probabilities. $N = 1000$, $K = 129$, $\alpha = 0.129$ with random initial conditions. For $p \approx 0.01$ the curves follow their complete graph counterparts, even though the number of connections is half as many, and travelling waves become unstable.

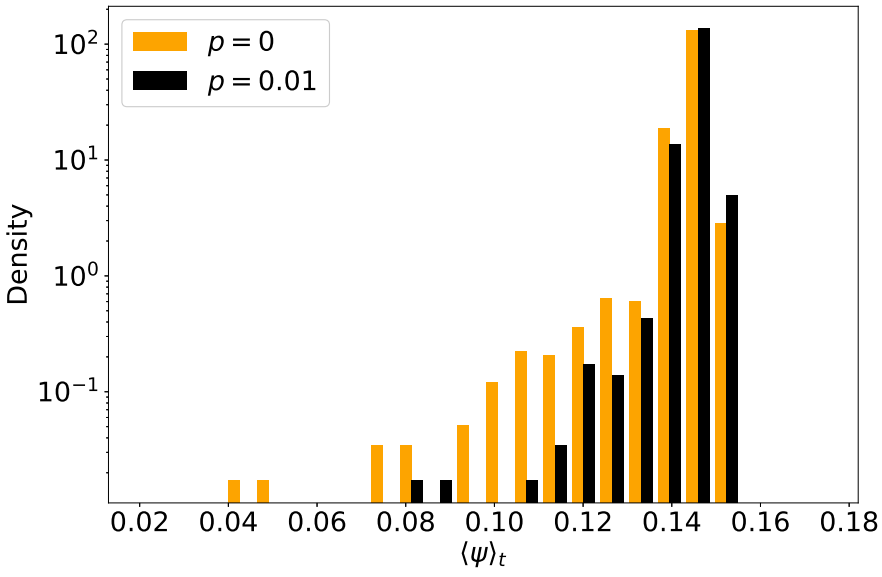

Figure 16 – (Color online) Networks with $N = 1000$, $K = 129$ and coupling $a = 2.5$. Histograms of $\langle\psi\rangle_t$ for 9000 realizations without rewiring (yellow), and 9000 realizations with rewiring probability $p = 0.01$ (black). The reduced frequency of small order-parameter values for $p = 0.01$ compared with $p = 0$ is evidence that rewiring destabilizes travelling waves, which are characterized by small values of ψ.

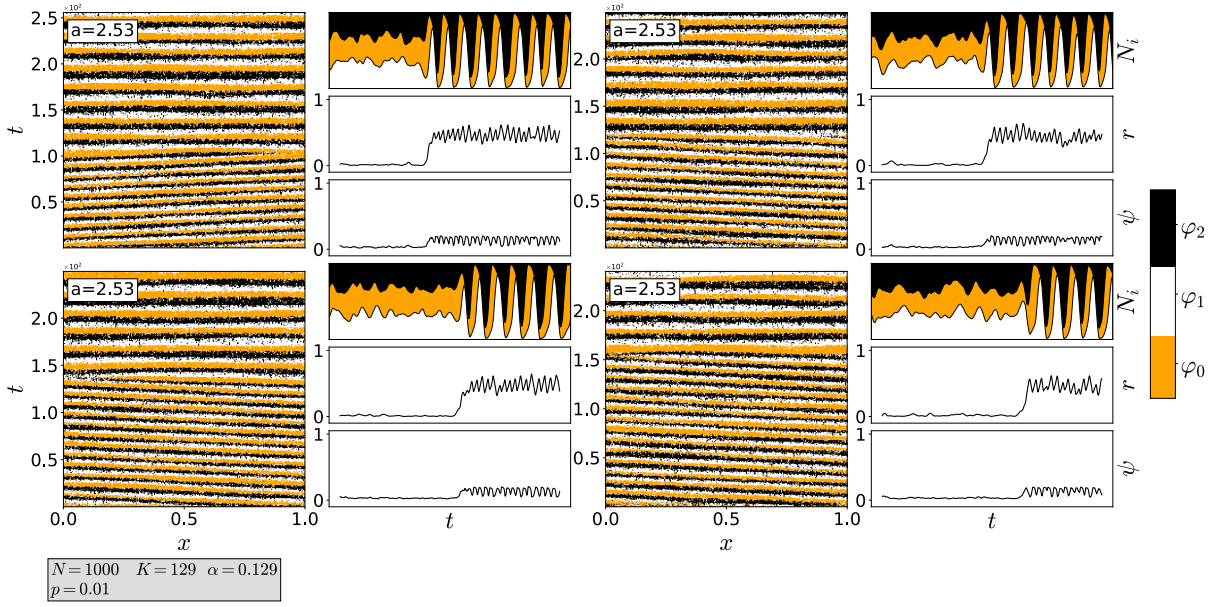

Figure 17 – Wave states for $N = 1000$, $K = 129$, $p = 0.01$ and $a = 2.53$. Only 0.04% of realizations (measured from 9000 realizations) with *random* initial configurations display traveling waves, which are also much more short-lived when compared to the $p = 0$ equivalent system.

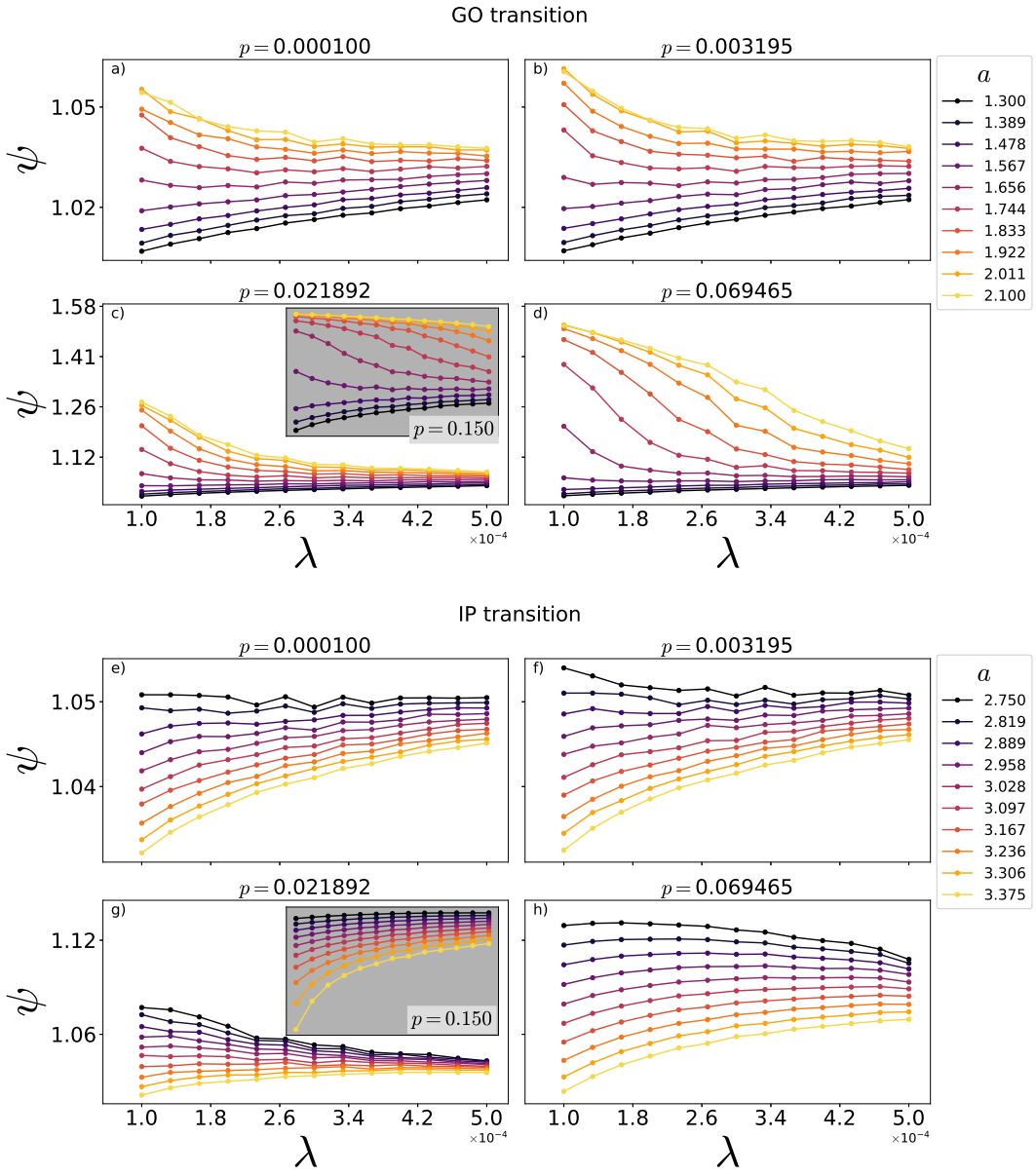

Figure 18 – (Color online) Order parameter ψ versus inverse system size λ for $\alpha = 0.00524$ and various values of rewiring probability p and couplings around the GO and IP transitions. Insets show the behavior for $p = 0.15$, the highest rewiring probability used.

2.6 Conclusions

We study the WCM model, a discrete-phase oscillator model exhibiting global synchronization and an infinite-period phase, on regular ring lattices and small-world networks. Each oscillator is coupled to a nonzero fraction α of the others, but the connectivity is in generally much smaller than for a complete graph. Our results support the conjecture that all three phases - disordered, globally synchronized, and infinite-period - appear for any nonzero connectivity α.

Surprisingly, travelling waves also appear in the small-α regime on regular ring lattices; such waves may represent a long-lived metastable state. (A previous study identified waves in the anti-coupling case [19].) In our studies travelling waves constitute only about 1.6% of the steady states reached from starting from *random* initial configurations, and are prone to decay into global oscillations due to fluctuations when system size is small. The introduction of long-range interactions through rewiring (i.e., using the Watts-Strogatz algorithm) can lead to synchronization without increasing the total number of connections. Rewiring also suppresses travelling waves by introducing long range interactions.

The fact that regular rings are capable of sustaining travelling waves for $a > a_c$ is surprising, showing that networks of oscillators might fail to synchronize even in the presence of nonlocal interactions and strong coupling, conditions which are sufficient for the synchronization on hypercubic lattices of dimensions greater than 2 as well as on the complete graph. This raises the possibility that WMCs admit wave-like steady states on cubic lattices, similar to oscillations observed in the two-dimensional Belousov–Zhabotinsky reaction.

Several other questions remain open for future study, for example, whether travelling waves represent a stable phase for some range of parameters, or are always metastable, and whether waves of wavelength smaller than the system size N are possible. We have sketched a phase diagram for ring lattices, but detailed information for the small-connectivity regime is lacking. Since the model exhibits a pair of continuous phase transitions, it is of interest to develop a full scaling picture, including the effect of ordering fields conjugate to the order parameters. Finally the question of what simple external perturbations are capable of destroying synchronization or the symmetry-broken phase may be of some practical interest.

3 Mean-field theory for small-world networks

In this chapter we develop a mean field (MF) theory for the coupled oscillator dynamics with three discrete phase states in a system of N oscillators coupled in small-world networks as described by the Watts-Strogatz algorithm in section 2.5. We start by re-stating the dynamic rules, and then proceed to define the mean field and the continuous limit.

Table 1 – Definitions

N	Integer system size
K	Integer interaction range
a	Real coupling strength, $a \geq 0$
α	Interaction range as a fraction of system size $\alpha \equiv K/N$
p	Rewiring probability
$\gamma_j^x(t)\|\gamma_j(x,t)$	Transition rate out of state j at position x and time t
$P_j^x(t)\|P_j(x,t)$	Probability that an oscillator at x is in state j at time t

An oscillator is described by its discrete phase, which can be imagined as a clock hand which abruptly jumps from noon to 4pm, then to 8pm and back to noon. Note that, as in a clock, the phase can only move forward, looping back on itself after three jumps. These jumps occur randomly, but with a well defined transition rate. When two oscillators interact, the rate of transition may change depending on the relative phase between the two units.

To describe the phase and interactions, we adopt a convention: oscillators are arranged in a circle and numbered from 1 to N (see figure 19). The superscripts then refer to the oscillator position while the subscripts denote a phase state from 1 to 3. Given a graph in which nodes represent phase oscillators labeled by x, the unit at position x is described by its phase

$$\begin{aligned} \phi^x &= 2\pi(j-1)/3 \\ j &\in \{1,2,3\} \end{aligned} \tag{3.1}$$

where $j \in \{1,2,3\}$ is the state of unit x. Since transitions can only occur in one direction, the stochastic rate of transition from j to $j+1$ is written just as γ_j^x, and its behavior is chosen to be of an exponential form:

$$\gamma_j^x(t) = \omega^x \exp\left[a\frac{n_{j+1}^x(t) - n_j^x(t)}{n^x}\right] \qquad x = 1, \ldots, N \tag{3.2}$$

where ω^x is its natural (uncoupled) frequency, $n_j^x(t)$ is the count of how many of its neighbors are in state j, and n^x is its total number of neighbors.

Let the probability of finding the unit at position x in state j at time t be $P_j^x(t)$. Since there are only three possible states we have the constraints $P_1^x(t) + P_2^x(t) + P_3^x(t) = 1$ for all x and t. The rate of change of the probabilities can be written in terms of the transition rates $\gamma_j^x(t)$, giving us $2N$ equations of motion:

$$\begin{aligned} \dot{p}_1^x(t) &= \gamma_3^x(t)(1 - P_1^x(t) - P_2^x(t)) - \gamma_1^x(t)P_1^x(t) \\ \dot{p}_2^x(t) &= \gamma_1^x(t)P_1^x(t) - \gamma_2^x(t)P_2^x(t) \qquad\qquad x = 1, \ldots, N \end{aligned} \tag{3.3}$$

The first terms in the RHS of (3.3) represent the fluxes of probability from oscillators in the preceding state, which can advance one phase state and increase the populations of oscillators in states 1 and 2 respectively. The second (negative) terms represent the fluxes generated by the oscillator leaving the considered state, and thus reducing its population. The dynamics can take place on any arbitrary network that defines the coupling between oscillators. Previous work has explored hyper-cubic lattices and complete graphs as well as regular ring graphs [1, 18, 19].

Here we start by focusing on ring lattices, which will be the starting point for generating small-world networks. Ring lattices are constructed by arranging N oscillators in a circle, and then for each unit, adding K clock-wise connections to the next K units in the circle, resulting in a circular shape with NK total connections. The result of this process for $N = 12$ and $K = 2$ is shown in figure 4 of chapter 2, as well as for $N = 16$, $K = 2$ in figure 19 right.

To generate a small-world network from a ring graph we perform a *rewiring* procedure. It visits each existing connection exactly once, and with a probability p exchanges the clockwise vertex of this connection for a randomly selected node in the network, avoiding duplicate connections or self connections. This will be described in detail when deriving the MF approximation for small-world networks.

3.1 The local average field in the discrete case

To define the local average field, we introduce a *local order parameter* ν identified by the fractions in the exponent of equation (3.2) at a fixed time t. It is a measure of the synchrony between oscillators which are coupled to the oscillator at position x.

$$\nu_j^x(t) \equiv \frac{n_j^x(t)}{n^x}, \tag{3.4}$$

the transition rates are now written as,

$$\gamma_j^x(t) = \omega^x \exp\left[a(\nu_{j+1}^x(t) - \nu_j^x(t))\right]. \tag{3.5}$$

The quantity ν_j^x describes the fraction of oscillators connected to x that are in state j, and thus also satisfies the constraint $\nu_1^x + \nu_2^x + \nu_3^x = 1$.

In the large-N limit, we approximate ν_j^x in equation (3.5) by its time-dependent average over realizations, $\left\langle \nu_j^x(t) \right\rangle$. When the rewiring probability $p = 0$, it was shown that for the chosen form of the coupling, the variance $\mathrm{Var}[\nu_j^x]$ is proportional to $1/N$ [19]. In the case of small-world networks ($0 < p \leq 1$) it is unfeasible to explicitly calculate the variance of the local order parameter, but in section 3.1.3 we develop arguments that support the validity of this mean-field approximation by performing partial calculations, and in chapter 4 we also perform numerical simulations for finite systems.

If fluctuations are small compared to the deterministic drift described by the MF approach the assumptions become better, but a quantitative description may suffer from imprecision when compared to simulation results. With this in mind, the MF transition rates become:

$$\gamma_{j,MF}^x = \omega^x \exp\left[a\left(\left\langle \nu_{j+1}^x(t) \right\rangle - \left\langle \nu_j^x(t) \right\rangle\right)\right] \tag{3.6}$$

For regular rings, the total number of neighbors of every site is fixed, $n^x = 2K$, but when dealing with rewired networks n^x becomes a random variable which may assume different values in different realizations, making $\left\langle \nu_j^x(t) \right\rangle$ trickier to calculate.

The equations of motion in the MF approximation are obtained by replacing the instantaneous transition rates in equation (3.3) by their mean-field values.

$$\begin{aligned} \dot{P}_1^x(t) &= \gamma_{3,MF}^x(1 - P_1^x(t) - P_1^x(t)) - \gamma_{1,MF}^x P_1^x(t) \\ \dot{P}_2^x(t) &= \gamma_{1,MF}^x P_1^x(t) - \gamma_{2,MF}^x P_2^x(t) \end{aligned} \tag{3.7}$$

We are left with the task of calculating $\left\langle \nu_j^x(t) \right\rangle$ in terms of the probabilities $P_j^x(t)$ such that 3.7 is an autonomous system. For that we define the indicator variable $D^{xx'}$, indicating the presence (or absence) of coupling between nodes x and x' in a graph.

3.1.1 Mean field value of the local order parameter

The expressions for $\nu_j^x(t)$ in the discrete case can be written in terms of the indicator variables $D^{xx'}$:

- Let $D^{xx'}$ be defined as

$$D^{xx'} = \begin{cases} 1 & \text{if the connection } x,x' \text{ exists} \\ 0 & \text{otherwise} \end{cases} \tag{3.8}$$

- Let x denote some position in the lattice for which we wish to know the local order-parameter value.
- Let j denote the state for which we wish to measure ν_j^x.

Then:

$$\begin{aligned} n_j^x(t) &= \sum_{x'=1}^{N} D^{xx'}\delta(j, j'(t)) \\ n^x &= \sum_{x'=1}^{N} D^{xx'} \end{aligned} \tag{3.9}$$

where j' is the state of the oscillator at position x' at time t and $\delta(j, j'(t))$ is the usual Kronecker delta defined by $\delta(j, j') = 1$ if $j = j'$ and 0 otherwise. The average over realizations then become

$$\left\langle \nu_j^x(t) \right\rangle = \sum_{x'} \left\langle \frac{D^{xx'}\delta(j, j'(t))}{\sum_{x''} D^{xx''}} \right\rangle,$$

or,

$$\left\langle \nu_j^x(t) \right\rangle = \sum_{x'} \left\langle \frac{D^{xx'}}{\sum_{x''} D^{xx''}} \right\rangle \langle \delta(j, j'(t)) \rangle \,. \tag{3.10}$$

Equation (3.10) introduces the principal MF approximation, treating $\delta(j, j'(t))$ as independent of $D^{xx'}$, implying the dynamics is described by the "average connectivity" between oscillators on the graph. This approximation becomes more accurate when the probability of rewiring p approaches zero, which is true for a large number of networks in the small-world regime, as seen in figure 14 of chapter 2. When $p = 0$ we can restrict the summation over connected sites, from $(x - K)$ to $(x + K)$, recovering the MF proposed by Escaff *et al.* [19] for regular rings.

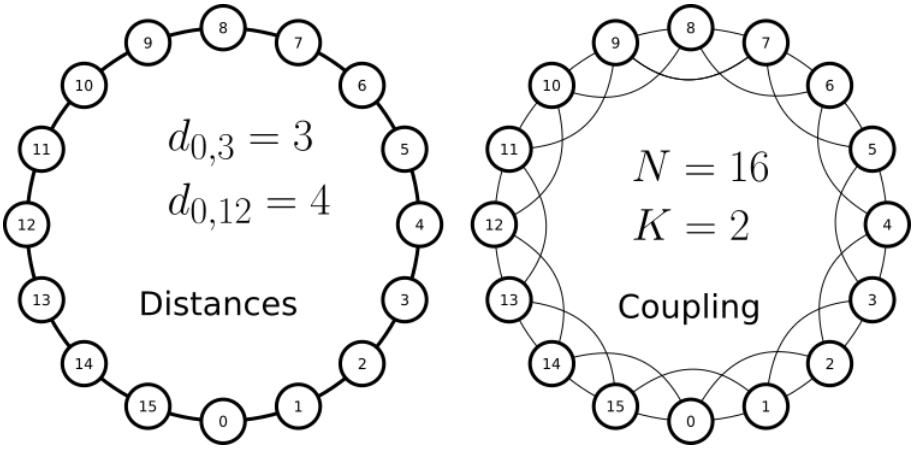

Figure 19 – **Left:** Definition of distance $d_{xx'}$ between sites x and x'. The distance $d_{xx'}$ is considered on the one dimensional chain and does not take into account the connections that determine the coupling.
Right: Example of the initial ring lattice before any rewiring is performed, where the lines represent the coupling between units.
The dynamics takes place on a periodic one-dimensional system with interaction range K.

The average $\langle \delta(j, j'(t)) \rangle$ is identified with the probability of finding site x' in state j at time t: $\langle \delta(j, j'(t)) \rangle \equiv P_j^{x'}(t)$, and we are left with the task of calculating $\left\langle D^{xx'} / \sum D^{xx'} \right\rangle$. In order to unpack this expression we need a detailed description of the rewiring algorithm, which ultimately dictates the connectivity of the final graph.

3.1.2 Rewiring algorithm

Here we give a detailed description of the rewiring algorithm in order to justify our expressions for the probability of connections in the final graph, which dictate the dynamics. It considers each connection in the starting graph exactly once, and with probability p it tries to swap one of its vertices for another randomly selected node in the network, avoiding double connections or self-connections. Detailed instructions on how it is implemented are written in the following pseudo-code.

```
Given a ring lattice with N nodes and range K do:
for z from 1 to K:
  for x from 1 to N:
    with probability p do:
      sample a uniform integer r from 1 to N
      if ( r == x ) or ( connection (x, r) already exists ):
        do nothing
      else:
        remove the connection (x, x+z)
        add the connection (x, r)
```

To determine the probability that the connection (x, x') exists in the rewired graph, we introduce the notion of distance between nodes x and x'. Let this be denoted by $d_{xx'}$, and the distance defined in the one-dimensional chain as illustrated in figure 19. Due to the periodic condition $x \mapsto x + N$ on the boundaries, no distance can be greater than $N/2$, and thus $d_{xx'}$ is formally defined as:

$$d_{xx'} = \begin{cases} |x - x'| & \text{if } |x - x'| \leq N/2 \\ N - |x - x'| & \text{if } |x - x'| > N/2 \end{cases} \tag{3.11}$$

To calculate the average values $\left\langle D^{xx'} \right\rangle$ we consider two cases: $d_{xx'} \leq K$, the **close case**, and $d_{xx'} > K$, the **far case**. The reasoning is that:

- If the initial distance between two nodes is less than or equal to K, then by construction of the ring graph they start out connected. The condition that this connection exists in the final graph is that it was never removed in the first place, or it could have been removed and then subsequently reformed.
- On the other hand, sites with $d_{xx'} > K$ start out disconnected, and thus a connection (x, x') can only result from one of its vertices being rewired that way.

With a little thought regarding the rewiring procedure, one will agree that if it produces any connection, it is guaranteed to be present in the result. Conversely, if it fails to break an initial connection, that connection is also guaranteed to exist in the final graph.

Far case

Here we derive the probability of existence of a connection between x and x' when $d_{xx'} > K$. Since the algorithm tries to swap (with probability p) the clockwise node of an

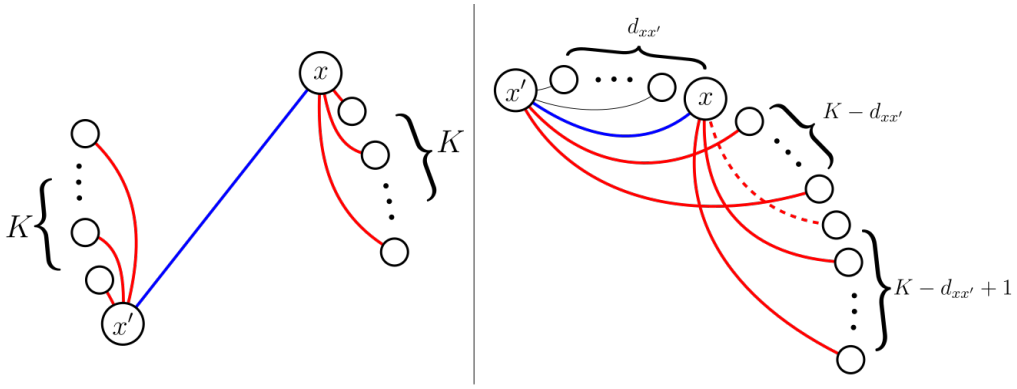

Figure 20 – The presence of the connection (x, x'), in **blue**, in a small-world network generated from the Watts-Strogatz algorithm can only be the result of the rewiring of a **red** connection. On the left side, the **far** case, $2K$ connections may contribute to the formation of (x, x'). On the **near** case (right side), the original connection may either be left untouched or, in case it is initially broken, it might be wired again by any of the remaining $2(K - d_{xx'}) + 1$ solid red connections.

initial connection, the only connections that could possibly have broken to form (x, x') are the K clockwise neighbors of x, and the K clockwise neighbors of x', as illustrated in the left panel of figure 20. If any of these $2K$ events take place, (x, x') is guaranteed to exist. Thus, $P(D^{xx'} = 1)$ is the probability that at least one forming event took place, which is just the complement of the probability that *no* such event took place.

$$P(D^{xx'} = 1) = 1 - \left(1 - \frac{p}{N}\right)^{2K} \qquad \text{for} \quad d_{xx'} > K \tag{3.12}$$

In equation (3.12), the probability that a connection rewires to (x, x') is the probability that it breaks times the probability of selecting the other vertex, which is just p/N. Therefore, the probability that a connection *does not* rewire to (x, x') is the complement $1 - p/N$. The probability that *none* of the $2K$ connections generate (x, x') is then $(1 - p/N)^{2K}$, and the probability that at least one of them *does* generate it is the complement again.

Near case

The near case is given by $d_{xx'} \leq K$. When considering the probability of existence for such shorter range connections, things get more complicated because the exact solutions depend on the choice of the starting point of the rewiring procedure. Consider the case shown in figure 21 for interaction range $K = 1$.

If the rewiring process starts at point A, then rewiring of connection C2 contributes to the probability that C1 is present in the final graph. On the other hand, if the rewiring

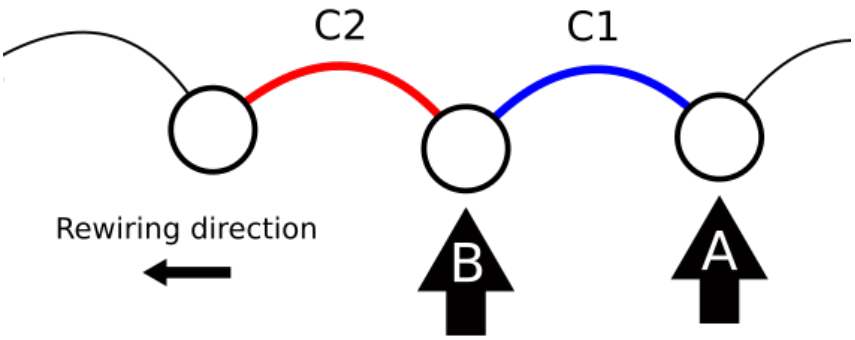

Figure 21 – Rewiring of connection C2 may or may not contribute to the probability of existence of connection C1. If the rewiring process starts at A, then C2 may be rewired into C1 if it was initially broken. On the other hand, if the starting point is B, connection C2 can never be rewired to C1 because the later will always be present at the time of rewiring C2.

starts at point B, then C2 does not contribute to the probability of existence of C1. Therefore C1 has a higher probability of existing for a rewiring that started at A as opposed to one that started at B. Luckily for our purposes the order dependence only happens for the first connection of length $d_{xx'}$ (dashed red line on right of figure 20), since for subsequent connections (solid red lines on same figure) the pair (x, x') will already have been considered by the algorithm, and any forming event from that point guarantees the existence of the connection (x, x').

To avoid order dependence, we will assume the problematic event contributes the same amount as subsequent events to the probability of existence of the considered connection. Thus, all $2K - 2d_{xx'} + 1$ events contribute equally to $P(D^{xx'} = 1)$, which is written as:

$$P(D^{xx'} = 1) = 1 - p\left(1 - \frac{2K}{N}\right)\left(1 - \frac{p}{N}\right)^{2K-2d_{xx'}+1} \qquad \text{for} \quad d_{xx'} \leq K \tag{3.13}$$

As before, the expression is obtained by taking the complement of the probability that no event forms the connection (x, x'): the probability that the original connection is broken is $p(1 - 2K/N)$ (p times the probability of selecting a site which does not already have a connection with x). This is another approximation since the number of connections involving site x may change during the rewiring procedure, but because the later conserves the total number of connections it is at least justifiable for now (we later confirm it numerically). The term $(1 - p/N)^{2K-2d_{xx'}+1}$ accounts for the probabilities that no forming event occurs with the potential connections marked in red on the right side of figure 20.

3.1.3 The discrete average field

To check that the probabilities $P(D^{xx'})$ are valid, we performed Monte Carlo sampling of the small-world networks and plotted the relative frequencies obtained against the probabilities given by equations (3.12) and (3.13). The results are shown for various values of p and $\alpha \equiv K/N$ in figure 22, where good agreement is observed for all values of p and interaction range K with fixed $N = 1000$.

Note that since $D^{xx'}$ are binary variables with values 1 and 0 the probabilities $P(D^{xx'} = 1)$ are given by the average $\left\langle D^{xx'} \right\rangle$, resulting in

$$\left\langle D^{xx'} \right\rangle = \begin{cases} 1 - \left(1 - \frac{p}{N}\right)^{2\alpha N} & \text{if} \quad d_{xx'} > K \\ 1 - p\,(1 - 2\alpha)\left(1 - \frac{p}{N}\right)^{2(\alpha - \alpha')N + 1} & \text{if} \quad d_{xx'} \leq K \end{cases} \tag{3.14}$$

where we have used the definitions $\alpha \equiv K/N$ and $\alpha' \equiv d^{xx'}/N$, which are assumed to be constant as N scales with proportional K and $d^{xx'}$. When N is large, we use the property

$$\lim_{N\to\infty} \left(1 - \frac{p}{N}\right)^{2\alpha N + C} = e^{-2\alpha p}$$

to simplify the expression to

$$\left\langle D^{xx'} \right\rangle = \begin{cases} 1 - e^{-2\alpha p} & \text{if} \quad d_{xx'} > K \\ 1 - p\,(1 - 2\alpha)\, e^{-2(\alpha - \alpha')p} & \text{if} \quad d_{xx'} \leq K \end{cases} \tag{3.15}$$

Going back to equation (3.10), we wish to calculate the quantity $\left\langle \frac{D^{xx'}}{\sum D^{xx'}} \right\rangle$. To do this, we argue that $\mathrm{Var}\left[\sum D^{xx'}\right]$ is small, and thus $\sum D^{xx'} \simeq \left\langle \sum D^{xx'} \right\rangle$ which is a constant, allowing us to replace the average of the quotient by the quotient of the averages, leading to

$$\left\langle \frac{D^{xx'}}{\sum_{x'} D^{xx'}} \right\rangle \simeq \frac{\left\langle D^{xx'} \right\rangle}{\sum_{x'} \left\langle D^{xx'} \right\rangle} \tag{3.16}$$

For small-world networks, the parameter p tends to be small [4], as seen from figure 14. Thus, we take equation (3.15) and expand the exponential terms in powers of p around $p = 0$. Keeping up to first order in p results in:

$$\begin{aligned} \sum_{x'=1}^{N} \left\langle D^{xx'} \right\rangle = & \sum_{d_{xx'} > K} 2\alpha p \\ & + \sum_{d_{xx'} \leq K} (1 - p + 2\alpha p)\,, \end{aligned} \tag{3.17}$$

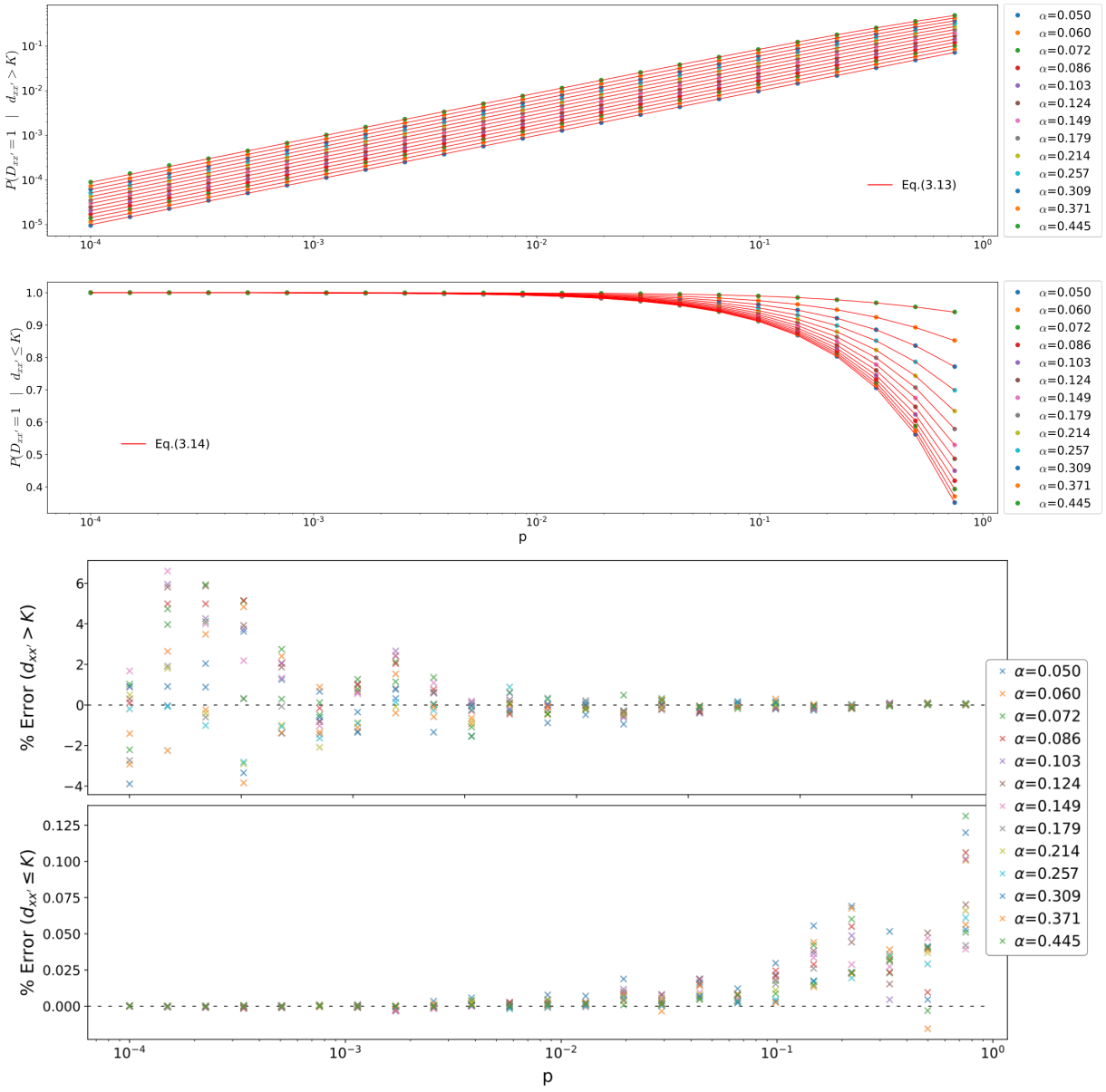

Figure 22 – Comparison between expressions for the probability of existence of connections as functions of rewiring probability p. Dots are obtained from Monte Carlo sampling of small-world networks produced by the Watts-Strogatz algorithm, solid red lines are equations (3.12) (top) and (3.13) (bottom).
System size $N = 1000$ with 50 realizations each. Note that when $p \to 0$ initially disconnected oscillators remain uncoupled while oscillators at distances $d^{xx'} \leq K$ remain coupled. The last two graphs depict the percentage deviation between sampling and predicted values, which is under 6% for connections longer than K and under 0.2% for shorter range connections.

Since the terms are now independent of x', and noting that there are $2K = 2\alpha N$ terms with distance $d^{xx'} \leq K$ and $N - 2K = N(1 - 2\alpha)$ terms with distance $d^{xx'} > K$, we obtain:

$$\sum_{x'=1}^{N} \left\langle D^{xx'} \right\rangle \simeq N(1-2\alpha)2\alpha p + 2\alpha N\,(1 - p + 2\alpha p)$$

which cancels out as

$$= \cancel{2\alpha N p} - \cancel{4\alpha^2 N p} + 2\alpha N - \cancel{2\alpha N p} + \cancel{4\alpha^2 N p}$$

giving,

$$\sum_{x'=1}^{N} \left\langle D^{xx'} \right\rangle \simeq 2K \tag{3.18}$$

This result is consistent with the previous statement that the average number of neighbors remains unchanged after the rewiring procedure, and also recovers previous results [19] for the case $p = 0$.

We now focus briefly on calculating $\mathrm{Var}\left[\sum D^{xx'}\right]$. The numerical analysis depicted in figure 22 shows that regarding the presence of connections in the final graph as independent events is a very good approximation. Thus, we can distribute the variance function inside the summation and ignore the covariance term, leading to:

$$\mathrm{Var}\left[\sum_{x'} D^{xx'}\right] = \sum_{x'} \mathrm{Var}\left[D^{xx'}\right] \tag{3.19}$$

where $\mathrm{Var}\left[D^{xx'}\right] = \left\langle \left(D^{xx'}\right)^2 \right\rangle - \left\langle D^{xx'} \right\rangle^2$, but since $D^{xx'}$ are indicator variables with outcomes 0 or 1, we have that $\left\langle \left(D^{xx'}\right)^2 \right\rangle = \left\langle D^{xx'} \right\rangle$ and therefore:

$$\mathrm{Var}\left[D^{xx'}\right] = \left\langle D^{xx'} \right\rangle - \left\langle D^{xx'} \right\rangle^2 \tag{3.20}$$

By making use of equation (3.15) and once more and expanding the exponentials around $p = 0$ gives:

$$\mathrm{Var}\left[D^{xx'}\right] = \begin{cases} 2\alpha p + \mathcal{O}(p^2) & \text{if } d^{xx'} > K \\ (1-2\alpha)\,p + \mathcal{O}(p^2) & \text{if } d^{xx'} \leq K \end{cases} \tag{3.21}$$

which finally gives us the result

$$\sum_{x'=1}^{N} \mathrm{Var}\left[D^{xx'}\right] \simeq \sum_{d^{xx'}>K} 2\alpha p + \sum_{d^{xx'}\leq K} (1-2\alpha)\,p$$

or,

$$\mathrm{Var}\left[\sum_{x'} D^{xx'}\right] = (1-2\alpha)\,4\alpha pN + \mathcal{O}(p^2)N \tag{3.22}$$

The resulting variance is proportional to Np, and thus for large N it grows without bound. Nonetheless, it may be regarded as sufficiently small when compared to other system properties which are independent of p and, with these last considerations, we proceed to write the expression for the average of the local order parameter as:

$$\left\langle \nu_j^x(t) \right\rangle = \frac{1}{2K} \sum_{x'} \left\langle D^{xx'} \right\rangle P_j^{x'}(t) \tag{3.23}$$

where $P_j^{x'}(t) \equiv \langle \delta(j, j'(t)) \rangle$ is the probability that the state j' of the oscillator at position x' is equal to j at time t. Using equation (3.15) and substituting into (3.23) results in the MF expression:

$$\left\langle \upsilon_j^x(t) \right\rangle = \underbrace{\frac{p}{N} \sum_{x'=1}^{N} P_j^{x'}(t)}_{\text{Global}} + \underbrace{\frac{1-p}{2K} \sum_{x'=x-K}^{x+K} P_j^{x'}(t)}_{\text{Local}} \tag{3.24}$$

where we have completed the global sum by adding and subtracting the missing gap $x'-K$ and $x'+K$.

We see that the effect of the rewiring process is to induce a global coupling component, while the coupling inside the initial range $2K$ is reduced by a factor $(1-p)$. In the limit of $p \to 0$, equation (3.24) recovers the MF previously derived by Escaff *et al.* for regular ring lattices [19]. We also note that the limit $p \to 1$ yields an intuitive result, even if only qualitatively so: when the network is fully random ($p = 1$), the local term vanishes, resulting exclusively in a global term. This is expected from our early assumption that the dynamics are governed by the average connectivity, since for random networks every connection has the same average connectivity value.

3.2 Continuous limit

In the previous section the discrete MF was derived by taking the limit $N \to \infty$ while keeping the ratio $\alpha \equiv K/N$ fixed. We now proceed to take the continuous limit of (3.24) by mapping the oscillators indices from 1 to N to the semi-open interval $[0, 1)$ in the reals. The indexes $x, x' \in \{1, ..., N\}$ become position coordinates $x, x' \in [0, 1)$ and therefore $\nu_j^x(t) \to \nu_j(x, t)$ where j still represents the state of the unit at x with $j \in \{1, 2, 3\}$. Analogously, the expression for the probability of finding the oscillator at x

in state j is now the density $P_j(x,t)$. The periodic conditions for any function of position x becomes $f(x) = f(x+1)$. As for the sums we now have

$$\begin{aligned} \frac{1}{N}\sum_{x'=1}^{N} &\to \int_0^1 dx' \\ \frac{1}{2K}\sum_{x'=-K}^{K} &\to \frac{1}{2\alpha}\int_{-\alpha}^{\alpha} dx' \end{aligned} \tag{3.25}$$

which leads us to the continuous expression for $\nu_j(x,t)$:

$$\nu_j(x,t) = p\int_0^1 P_j(x',t)dx' + \frac{1-p}{2\alpha}\int_{x-\alpha}^{x+\alpha} P_j(x',t)dx'. \tag{3.26}$$

The transition rate from state j to $j+1$ for an oscillator at position x in the continuous MF limit is then given by rewriting equation (3.5) with the notation $\gamma_j^x(t) \to \gamma_j(x,t)$ and using (3.26) in place of ν_j^x:

$$\gamma_j(x,t) = \omega(x)\exp\left\{a\left[\nu_{j+1}(x,t) - \nu_j(x,t)\right]\right\} \tag{3.27}$$

where $\omega(x)$ is the uncoupled frequency of the oscillator at x, sampled from some unimodal symmetric distribution g.

The set of $2N$ master equations (3.3) that describe the time evolution of probabilities reduce to just 2 equations for the now spatially distributed probability $P_j(x,t)$. Again we have the condition $P_1(x,t) + P_2(x,t) + P_3(x,t) = 1$ so that we only need two equations to describe the probabilities of all three states. The equation of motion for state j is then written as

$$\dot{P}_j(x,t) = \gamma_{j-1}(x,t)P_{j-1}(x,t) - \gamma_j(x,t)P_j(x,t) \qquad x \in [0,1) \tag{3.28}$$

The solutions of equations (3.28) thus describe the predicted behaviors of sufficiently large populations of oscillators, and can be compared to simulation.

3.3 Solutions of the continuous mean-field equations

Equations (3.27) and (3.28) represent the MF approximation for rewired ring lattices. One solution to this system is $P_1(x,t) = P_2(x,t) = 1/3$, called the *quiescent* solution. To see this, note that from equation (3.26) we have $\nu_1(x,t) = \nu_2(x,t)$ when

the probabilities are the same, and therefore $\gamma_1(x,t) = \gamma_2(x,t) = \gamma_3(x,t) = \omega(x)$ from equation (3.27). The *quiescent* solution is stable when the coupling strength a is below some critical value a_c that depends on the couplings and whose lowest value is attained for the complete graph, with $a_c = 1.5$. The threshold a_c marks a Hopf bifurcation[1]type transition for graphs that support global oscillations [1] [4] [15] [17]. When the coupling a is larger than the critical value a_c the *quiescent* solution becomes unstable and self-organization takes place, usually in the form of global synchronization, but does not necessarily mean they are stable in the mathematical sense.

In chapter 4 we explore simulations on small-world networks with strong coupling that do not always lead to global oscillations. Depending on initial conditions and the intrinsic noise, the system may exhibit a travelling wave, displaying only local synchronization. Following a similar analysis by Escaff et al. [19], we investigate such a wave solution by perturbing the *quiescent* state with a waveform and then checking what happens to the time evolution of the amplitude of said perturbation, which we modulate by some arbitrary parameter ϵ_j:

$$P_j(x,t) = 1/3 + \epsilon_j e^{ikx+\lambda t} \tag{3.29}$$

where $i = \sqrt{-1}$, $k \in \mathbb{R}$ and $\lambda \in \mathbb{C}$. The periodic condition $P_j(0,t) = P_j(1,t)$ implies that $k = 2m\pi$ for an integer m. Assuming (3.29) at $t = 0$ to be the initial configuration of the system, the goal is to identify whether there are any conditions on the model parameters that allow for the wave amplitude to grow, which happens when $\mathrm{Re}[\lambda] > 0$. Thus, for wave solutions we have

$$\dot{P}_j(x,t) = \lambda \epsilon_j e^{ikx+\lambda t} \tag{3.30}$$

and for $\nu_j(x,t)$ (equation (3.26)) the global component vanishes, due to the periodic condition $k = 2\pi m$, and we get:

$$\nu_j(x,t) = \frac{p}{3} + p\epsilon_j e^{\lambda t} \cancelto{0}{\int_0^1 e^{ikx'} dx'} + \frac{1-p}{3} + \frac{1-p}{2\alpha}\epsilon_j e^{\lambda t} \int_{x-\alpha}^{x+\alpha} e^{ikx'} dx'$$

$$\nu_j(x,t) = \frac{1}{3} + (1-p)\frac{\sin k\alpha}{k\alpha}\epsilon_j e^{ikx+\lambda t} \tag{3.31}$$

equation (3.31) can now be substituted in (3.27) to obtain the transition rate for the wave solution:

[1] A Hopf bifurcation occurs when a periodic solution arises around an equilibrium point as some parameter varies. Here, the oscillations arise around the *quiescent* solution as a increases beyond a_c.

$$\gamma_j(x,t) = \omega(x)\exp\left[a(1-p)\frac{\sin k\alpha}{k\alpha}(\epsilon_{j+1}-\epsilon_j)e^{ikx+\lambda t}\right] \tag{3.32}$$

Substituting equations (3.29),(3.30) and (3.32) into equations (3.28) yields the conditions under which the wave solution may exist. We introduce here the notations $W \equiv ikx + \lambda t$ and $\hat{a} \equiv a(1-p)\frac{\sin k\alpha}{k\alpha}$ for brevity:

$$\lambda\epsilon_j e^W = \omega(x)e^{\hat{a}(\epsilon_j-\epsilon_{j-1})e^W}\left(1/3+\epsilon_{j-1}e^W\right) - \omega(x)e^{\hat{a}(\epsilon_{j+1}-\epsilon_j)e^W}\left(1/3+\epsilon_j e^W\right)$$

This can be reduced by using the approximation $e^x \approx 1+x$, $x \approx 0$ in the small-ϵ_j regime. Neglecting all the remaining terms in ϵ_j, of order 2 or higher, yields:

$$\begin{aligned}\lambda\epsilon_j \cancel{e^W} &= \omega(x)\left(1+\hat{a}(\epsilon_j-\epsilon_{j-1})e^W\right)\left(1/3+\epsilon_{j-1}e^W\right) - \omega(x)\left(1+\hat{a}(\epsilon_{j+1}-\epsilon_j)e^W\right)\left(1/3+\epsilon_j e^W\right)\\ &= \omega(x)\left(\epsilon_{j-1}-\epsilon_j+\frac{\hat{a}}{3}\left(2\epsilon_j-\epsilon_{j-1}-\epsilon_{j+1}\right)\right)\cancel{e^W}\end{aligned}$$

but the condition $P_{j-1}(x,t)+P_j(x,t)+P_{j+1}(x,t)=1$ implies $\epsilon_{j-1} = -\epsilon_j - \epsilon_{j+1}$ and thus:

$$\lambda = \omega(x)\left(\hat{a}-2-\frac{\epsilon_{j+1}}{\epsilon_j}\right) \tag{3.33}$$

Finally, setting $j=1$ and then $j=2$ gives us two independent equations which can be used to eliminate the ratio ϵ_1/ϵ_2 from equation (3.33) and solve for λ:

$$\lambda = \omega(x)\left(\hat{a}-2-\frac{\epsilon_2}{\epsilon_1}\right),$$

and

$$\begin{aligned}&\lambda = \omega(x)\left(\hat{a}-2+1+\frac{\epsilon_1}{\epsilon_2}\right),\\ &\Downarrow\\ &\lambda = \omega(x)\left(\hat{a}-\frac{3}{2}\pm\frac{1}{2}i\sqrt{3}\right).\end{aligned} \tag{3.34}$$

Equation (3.34) expresses the dispersion relation $\lambda(k,x)$, and thus the frequency of the travelling wave depends on position. If the natural frequencies were to form some macroscopic pattern throughout x, this analysis would predict local changes to the wave frequency as it travels around the system. But because $\omega \sim g$ for some symmetrical

unimodal distribution g, in the continuous limit the speed-ups and slow-downs cancel out and the result is dominated by the average value of g denoted by $\bar{g}$. This can be seen from the fact that, for any positive value δx we have:

$$\begin{gathered}\int_x^{x+\delta x} \omega(x')dx' = \bar{g} \\ \Downarrow \\ \int_x^{x+\delta x} \lambda(k,x')dx' = \bar{g}\left(\hat{a} - \frac{3}{2} \pm \frac{1}{2}i\sqrt{3}\right)\end{gathered} \tag{3.35}$$

And therefore, the local value of λ for an arbitrarily small neighborhood around x, for any x, is given by the average value $\bar{g}$. The perturbed solutions for sufficiently small values of ϵ_j are then written as

$$P_j(x,t) = \frac{1}{3} + \epsilon_j e^{\left(\hat{a}-\frac{3}{2}\right)\bar{g}t} e^{i\left(kx+\frac{\sqrt{3}}{2}\bar{g}t\right)} \tag{3.36}$$

where we have factored out $\mathrm{Re}(\lambda)$ to explicitly show the time dependence of the amplitude of the waveform. If this quantity is positive the wave amplitude grows without bound until higher-order terms start dominating, possibly leading to saturation and stable waves. If $\mathrm{Re}(\lambda)$ is negative then the perturbation will die out and the quiescent steady state will be reached. The fact that the dynamics only allows for one directional transitions (namely from j to $j+1$ cycling back to 1 when $j=3$) means $\bar{g} > 0$ always, and therefore $\mathrm{Re}(\lambda) > 0$ implies $\hat{a} > 3/2$ which is:

$$a(1-p)\frac{\sin(2\pi m\alpha)}{2\pi m\alpha} > \frac{3}{2}. \tag{3.37}$$

where m is an integer and α is the interaction range expressed as a fraction of system size. The derivation of equation (3.31) assumes $m \neq 0$ in order for the left integral to vanish, and thus the globally synchronized steady state ($m = 0$) is not described by equation (3.37). For a given value of α and some wave number m, the critical value for the coupling is given by setting an equality in equation (3.37):

$$a_c = \frac{3}{2}\frac{1}{(1-p)}\frac{(2\pi m\alpha)}{\sin(2\pi m\alpha)} \tag{3.38}$$

Thus, the critical value is a function of p, α, and the wave number m. If we fix p and α, which are continuous quantities, we can get a sequence of critical values by varying the wave number m. Table 2 shows a few such sequences for different choices of the

$\alpha\backslash m$	8	7	6	5	4	3	2	1
0.05	6.41	4.08	2.97	2.36	1.98	1.75	1.60	1.52
$\alpha\backslash m$	5	4	3	2	1	7	8	6
0.10	∞	6.41	2.97	1.98	1.60	-6.94	-7.93	-9.62
$\alpha\backslash m$	7	6	2	1	4	3	8	5
0.20	22.45	11.89	6.41	1.98	-7.93	-9.62	-25.66	$-\infty$

Table 2 – Critical values as a function of interaction range α (rows) and wave number m (columns). Rows are sorted by the value of the critical coupling. As interaction range increases, the destabilization of the wave numbers may change order when starting from no coupling ($a = 0$) and increasing/decreasing the coupling strength.

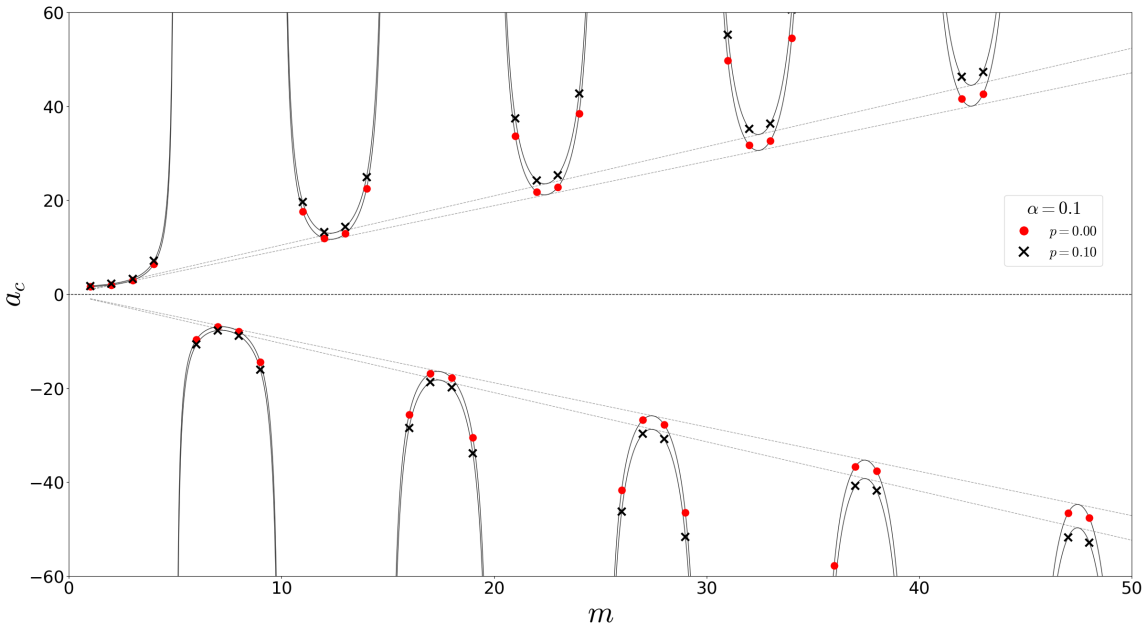

Figure 23 – Critical values for the coupling as the wave number increases for a fixed interaction range of $\alpha = 0.1$. The effect of increasing p is seen as a steeper slope for both positive and negative critical sequences.

connectivity range α and a rewiring probability of $p = 0$. Each row is sorted by decreasing critical values.

We see that if the coupling strength is decreased (increased) from 0 to more negative (positive) values, wave numbers become stable one by one. For example, if $\alpha = 0.2$ in table 2 and we decrease the coupling starting from 0, the first stable wave number is $m = 4$ at the critical value of $a_c = -7.93$. These are the results derived in the work of Escaff et al. [19] for the case of $p = 0$. In our extension to small-world networks, the effect of increasing p is to make the critical sequence increase or decrease more sharply, as illustrated in figure 23. A noteworthy aspect of these sequences of critical values is that,

for negative coupling, the system spontaneously self-organizes to a wave solution when the first negative critical value is reached. For positive coupling, the first stable solution is the globally synchronized one, with $m = 0$ and critical value of $a_c = 1.5$ [1,4,15,18]. Therefore, no wave solution will spontaneously form even when increasing the coupling to arbitrarily large values, since global synchrony is vastly more probable when starting the system from the quiescent initial state [4]. For real systems with finite size, we might expect that fluctuations can induce transitions between different wave numbers for positive values of the coupling parameter, which is indeed verified in simulations in chapter 4.

3.4 Conclusions

In this chapter we have derived a MF approximation for discrete coupled oscillators with natural frequency distribution $\omega \sim g$ on small-world networks generated by introducing coupling disorder into the regular ring networks. To obtain analytical results, and derive analogous expressions to previous work, we have restricted these to the regime of small disorder (p). It is also implicitly assumed that the behavior of a sufficiently large network will be approximated by the average behavior over different networks, since the building process for the small-world networks considered here is stochastic. For real finite systems, it is possible that some realizations of a small-world network will not produce these macroscopic behaviors, since fluctuations become more dominant as system size is decreased. Nonetheless, the theory predicts some properties that can be tested through simulation, such as the failure to achieve global synchrony even for large positive couplings depending on initial conditions and fluctuations, and the change in speed with which these waves travel if there are macroscopic patterns in the spatial distribution of the natural frequencies of the constituent phase oscillators.

4 Simulation: algorithm and results

In this chapter we present simulations performed with the objective of both gaining insight into the behavior of discrete-phase oscillators governed by the dynamics of (3.2) and (3.3), and to test predictions given by the MF description derived in chapter 3. Computations were carried out at the Statistics and Computation Service (SCS) cluster at the University of Michigan as well as local office and personal computers at UMICH and the Federal University of Minas Gerais. The source code is publicly available as a git repository[1] for viewing or recreating the data shown in this chapter. We start by defining the method chosen and discussing its implementation in detail, and then present the results.

4.1 Event-driven simulation

The system of discrete oscillators is a dynamical system in which each oscillator has three possible phases which can advance to the next state. The rates at which they transition depend on the relative states between each unit and its neighbors through equation (3.2), leading to the set of equations of motion (3.3). We seek to define an update rule for such a system that corresponds to solving these sets of equations.

The model structure over which the dynamics acts is the graph that defines the coupling between oscillators in which nodes represent oscillators and edges represent their coupling strength. Each node is labeled with a coordinate x and the value associated with it is its phase, encoded by the numbers 0, 1 and 2. The value associated with the edges is the coupling strength a, which is the same for every edge. The next step is giving every oscillator an initial phase, making the system well defined for the dynamical rules to act on it.

The implementation of choice for applying the dynamical rules is the event driven method, in which every update in the simulation is guaranteed to contain exactly one event, which in this case constitutes an oscillator advancing to the next phase. This method is adequate here because the overall transition rate of the system, given by the sum of all individual transition rates, can vary by several orders of magnitude depending on the configuration. Therefore, when there are few transitions happening in the system, the simulation doesn't slow down as would be the case in a simulation with fixed time step. Rather, it implicitly increases the time step such that there is always one event on every iteration. The converse is true for very active configurations, and the result is an algorithm

[1] https://github.com/KiloLiuton/event-driven-cpp-minimalist

that is faithful to the differential equations being modeled.

Calculating the simulation time step

Each oscillator has a transition rate γ^x, such that the expected time elapsed until its next transition is $(\gamma^x)^{-1}$. Since there are N such units in the system, the average waiting time τ for any such event to occur is given by $\tau = \Gamma^{-1}$ where $\Gamma \equiv \sum_x \gamma^x$ and therefore.

$$\tau(t) = \frac{1}{\sum_{x=1}^{N} \gamma^x(t)} \tag{4.1}$$

where we have explicitly written the time dependence of the transition rates to show that the time step in the simulation is also time dependent, increasing when the overall transition is small and slowing down when activity rises.

Algorithm

Now that we know how to obtain the time step τ, the average time elapsed until *some* oscillator transitions, we need to determine *which* one actually undergoes phase change. This is accomplished by sampling the transition rate distribution r given by

$$r(x, t_i) = \frac{\gamma^x(t_i)}{\Gamma(t_i)} \tag{4.2}$$

at the current simulation time t_i. After sampling, the selected position x is the label of the oscillator in the graph that will be updated to its next phase value. Once the state is updated, we also need to update the transition rate γ^x as well as $\gamma^{x'}$ where x' is a neighbor of x, allowing us to calculate the next time step $\tau(t_{i+1})$ and the new distribution $r(x, t_{i+1})$. With these definitions, the core loop procedure can be written as:

1. Sample the distribution $r(x, t_i)$ to obtain the transitioning oscillators label x
2. Update the phase $\phi^x(t_i) \to \phi^x(t_{i+1})$ and rate $\gamma^x(t_i) \to \gamma^x(t_{i+1})$
3. For all neighbors of x, update their respective rate values $\gamma^{x'}(t_i) \to \gamma^{x'}(t_{i+1})$
4. Increment the simulation time by $\tau(t_i)$ such that $t_{i+1} = t_i + \tau(t_i)$
5. If t_i is larger than the desired simulation time, stop, otherwise, repeat from 1.

Note that there is exactly one transition per iteration of the core loop, regardless of the value of $\tau(t_i)$.

Because calculating $\gamma(t_{i+1})$ requires comparing the new state $\phi(t_{i+1})$ to all of its neighbors, and because for each of them only the state of x has changed, there is some minor computational gain in combining steps 2 and 3, requiring a single loop through the neighbors of x.

4.2 Wave stability

Travelling waves are not the only stable solution on ring lattices. In the mean field description, the only way a system may reach this state is through a favorable initial condition. In real finite systems or in simulations this state may be reached spontaneously through fluctuations, even if the system is already at some other stable configuration. Nonetheless, in order to facilitate the stability study of wave solutions, we give the system an initial configuration that is already a wave. The MF description suggests that some combinations of interaction range α and rewiring probability p favors wave solutions through the equation for the critical coupling a_c for waves with wave number m:

$$a_c = \frac{3}{2}\frac{1}{(1-p)}\frac{(2\pi m\alpha)}{\sin(2\pi m\alpha)} \tag{4.3}$$

In chapter 2 we saw that the critical coupling value for transitions to global synchrony does not change with α (figure 6 for example). In the case of wave configurations the critical value changes with connectivity as well as wave number m. In addition, the introduction of disorder through the rewiring probability p also affects the stability of wave solutions according to equation (4.3) (at least for small p), but this effect is minor when compared to the effect it has on the onset of global synchrony or the infinite period transition, as seen from figure 15, where a very small amount of disorder causes wave solutions to quickly destabilize, giving way to global oscillations and infinite period steady states.

The stability of the lowest spatial frequency wave can be tested by setting $m = 1$ and performing simulations with parameters above and below the plane defined by equation (4.3) in the phase space defined by the coordinates (a, p, α), as seen in figure 24. In chapter 2 figure 12 we see that waves are superseded by global oscillations (GO) or the infinite period (IP) phases for sufficiently large α, and therefore not all points above the critical plane for waves in the phase space necessarily produce stable waves. The lack of expressions for the critical surfaces of the IP phase allows us to only sketch this surface based on the results of simulations, which show the onset of the IP phase to remain around its complete graph ($\alpha = 0.5$) value of $a \approx 3.1$ (see figure 15). In figures 25 and 26 we see some examples of the unfolding of the dynamics for six different points in parameter space. When $p = 0$ the phase separations are very clean and are in accordance with predictions. In the second

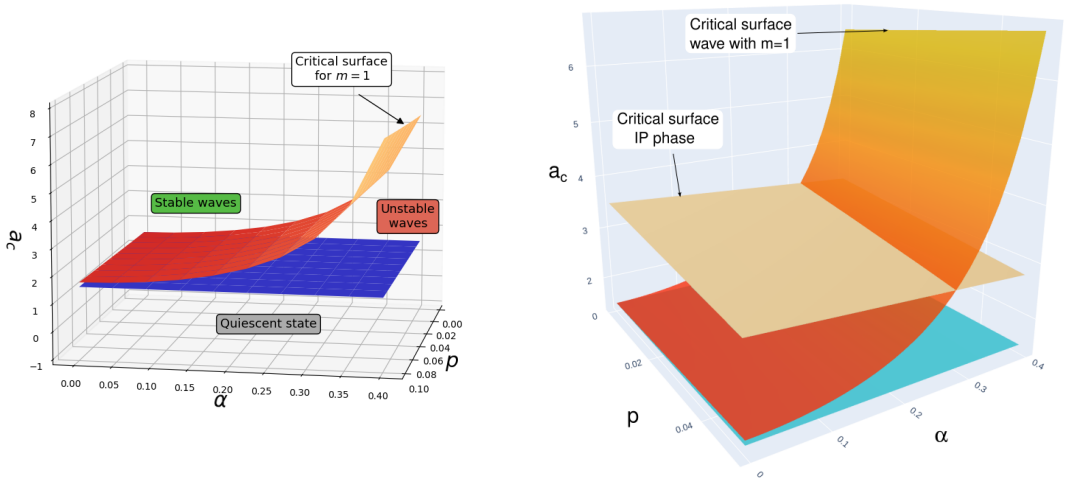

Figure 24 – Phase diagram in parameter space with coordinates (a, p, α), and surface defined by equation (4.3). In both graphs the blue plane has height of $a = 1.5$, representing the onset of globally synchronized solutions as coupling increases. On the left, points above the curved surface are expected to produce stable waves with wave number $m = 1$. Below this curve but above the plane, only globally synchronized oscillatory solutions are stable. On the right we have the same surfaces but with an additional plane representing a "sketch" of the critical surface with height $a \approx 3.1$ for the IP phase based on simulation results.

case, $p = 0.025$, a fairly large value, the separation becomes less abrupt, and there is a region where wave fronts may be created or annihilated spontaneously. To avoid such noisy phases one would need to simulate a larger system, as the previous scaling analysis (2.4) suggests, but any finite system will be subject to such fluctuations, due to competition between different wave numbers. In this scenario, the globally synchronized state can be thought of as a wave solution with wave number $m = 0$, which effectively removes the spatial component of the travelling wave, leaving only oscillations in time.

Spontaneous creation and annihilation of wave numbers

To illustrate how a system may fail to ever reach a steady state due to noise, we look at a simulation with parameters $(p = 0.005, \alpha = 0.12, a = 2.7)$ where the initial condition is a wave with wave number $m = 6$. Equation (4.3) tells us that the only stable wave numbers for these parameters are $m = 1$ and $m = 2$, in addition to global oscillations, $m = 0$. Figure 27 shows that indeed the wave number quickly drops, but after reaching $m = 0$ it starts oscillating around it. The value of $m = -1$ just means the wave is actually travelling to the opposite direction compared to $m = 1$, which is expected due to symmetry.

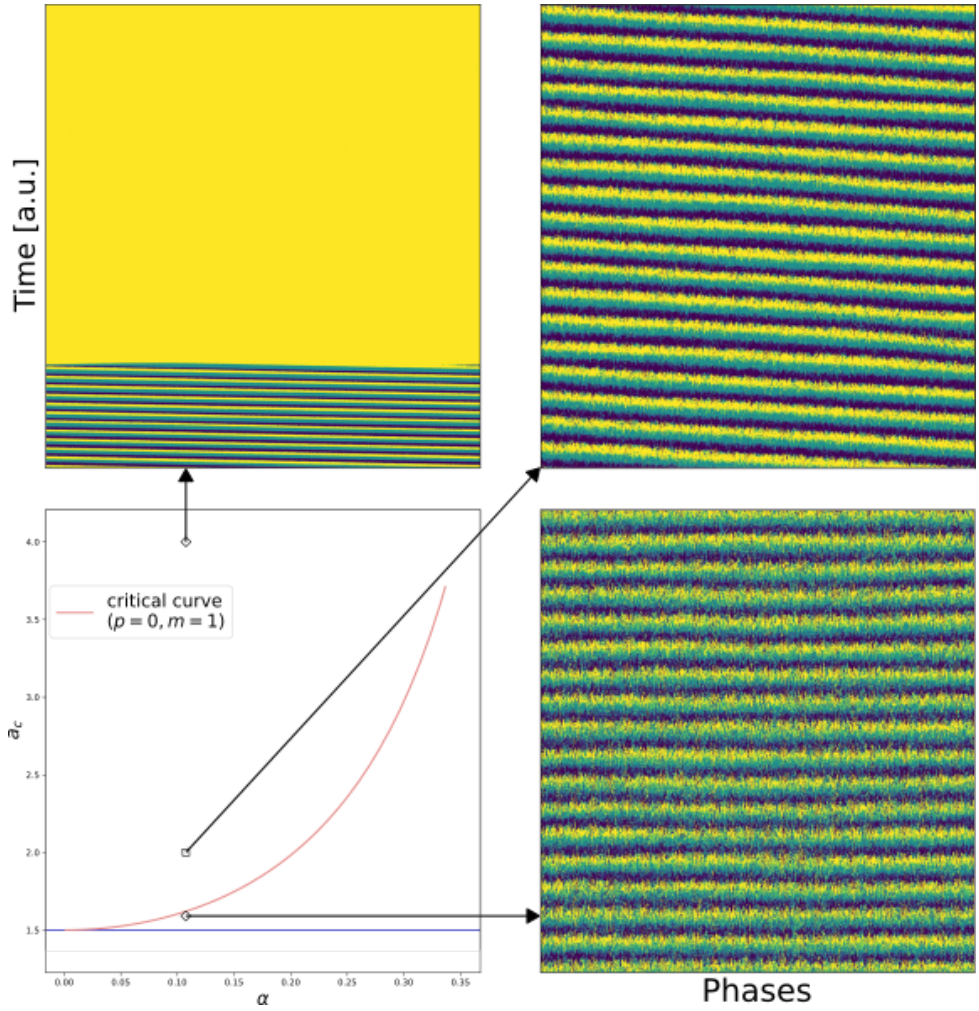

Figure 25 – Dynamic results from three different points in the phase space for $p = 0$. Below the critical curve but above the $a = 1.5$ line we observe global synchronized oscillations. Above the critical value for the wavenumber $m = 1$ we observe the stability of the corresponding travelling wave while for large coupling we see the onset of the infinite period transition where the period of global oscillations diverges.

4.3 Wave speed modulation

Finally, we show that the speed of the travelling wave may be modulated by introducing biases to the natural frequencies of the oscillators. In all previous simulations each natural frequency was sampled from a unimodal distribution with mean frequency around $\bar{\omega}$. In this section we introduce a spatial bias to the natural frequencies, such that faster oscillators are near $x = 0.5$ and the slower ones are located towards $x = 0$ and $x = 1$. In the regime of stable waves with $m = 1$, the time evolution for the phase configuration follows figure 28 for $a = 3.2$, $N = 8000$, $\alpha = 0.038$ and $p = 0.0128$. The inset on the top right shows the value of the derivative of the wavefronts dt/dx. Since the wave can travel to the left or right, we take the inverse relation and take the absolute value to get the magnitude of the wave speed, displaying a clear peak at the central region.

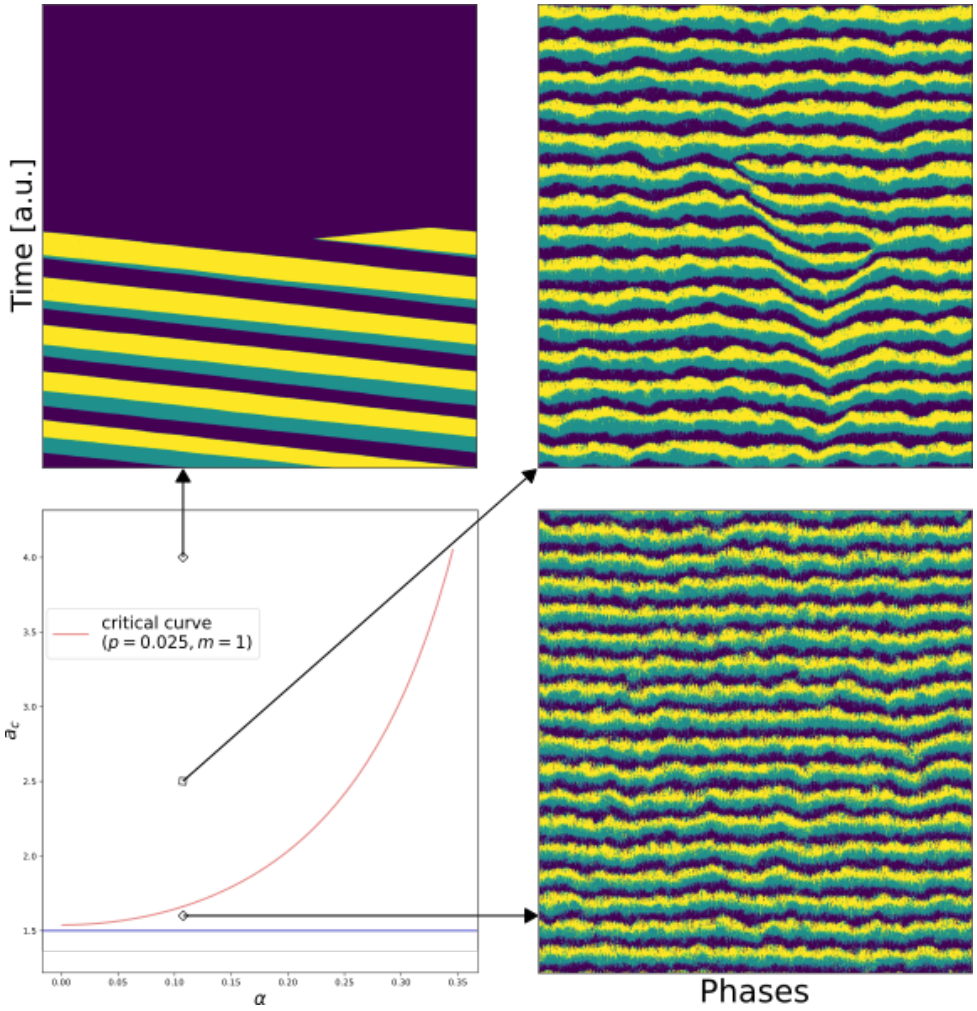

Figure 26 – Dynamic results from three different points in the phase space for $p = 0.025$. Below the critical curve but above the $a = 1.5$ line we observe some global synchrony. Above the critical value for the wavenumber $m = 1$ we observe intermittent stability of the corresponding wave, where the wave front is spontaneously created/annihilated while for large coupling we again see the onset of the infinite period transition.

4.4 Conclusion

Simulations show that finite systems are subject to the decay of wave solutions into global synchrony or the infinite period state, where the overall phase of the system remains fixed. Nonetheless, larger systems may display travelling waves pattern for arbitrarily long times. In addition, simulations also corroborate the MF result that wave solutions can persist even after the introduction of disorder through the rewiring process. Wave speed modulation by the natural frequencies is another result which was verified. Here, the natural frequencies of oscillators form a spatial pattern which speeds up the wave in the central region, causing the distortions observed in figure 28.

Another property of finite systems is that in regions of parameter space where

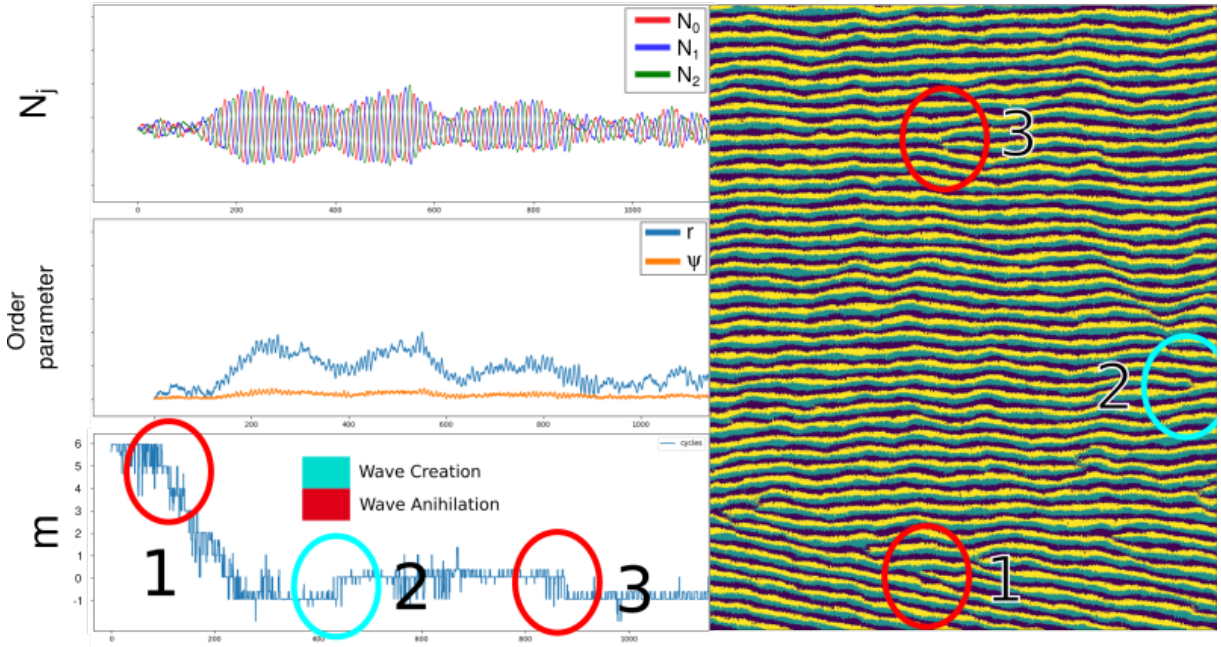

Figure 27 –

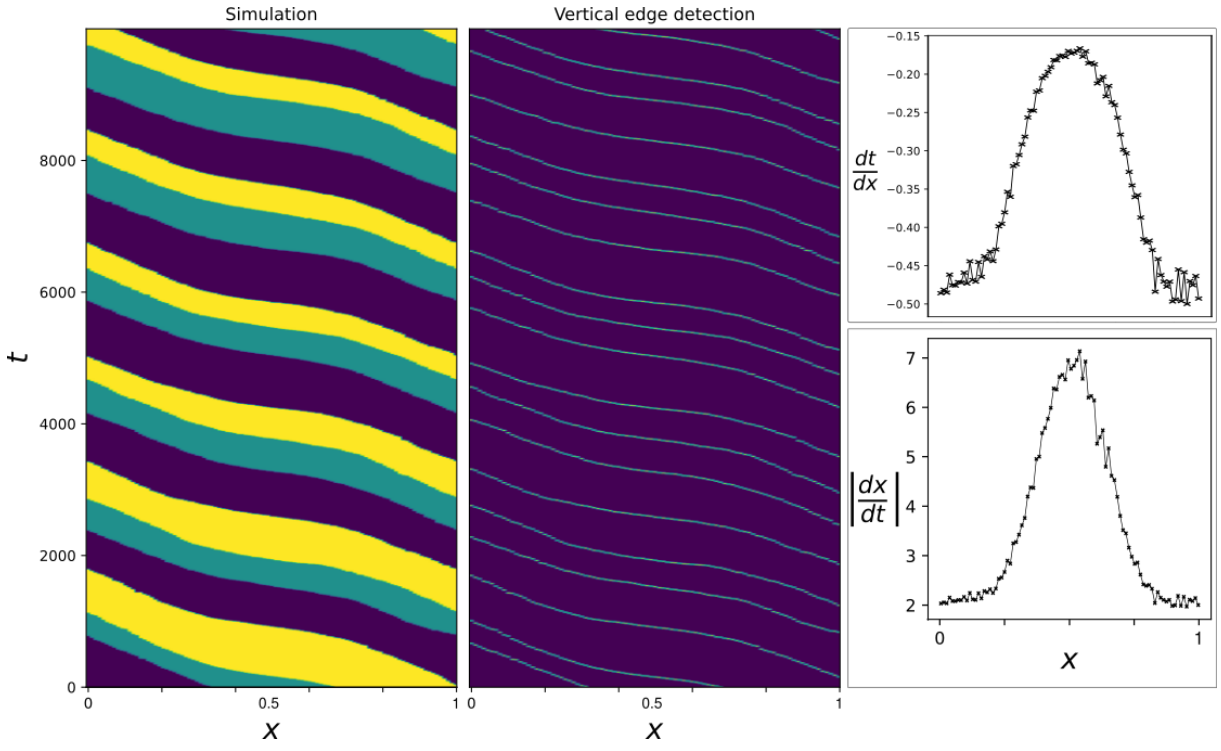

Figure 28 – Wave propagation in a system of size $N = 16000$ with $\alpha = 0.038$ and $p = 0.0128$ initialized in a wave configuration with $m = 1$. The wave speed is modulated by giving oscillators near $x = 0.5$ larger natural frequencies, following a curve of the form $\omega(x) = 1 + 2\sin^8 \pi x$ as opposed to $\omega(x)$ being a sample of some unimodal distribution g. In the central panel we see the result of a vertical edge detection whose results were used to calculate the derivatives. For each value of x in the right panels, the final derivative value is an average over all wave-fronts of the central panel.

there are more than one stable solution, the system may spontaneously transition between them, as is seen if figures 27 and 26. The transitions between wave numbers appear as semi-plane defects on the t vs x graphs and they can happen in any direction. In this scenario global oscillations are just the special case where the wave number $m = 0$, and the system may transition out of it spontaneously.

5 Conclusions and perspectives

Starting from the Wood Cyclic Models, we have extended the investigations to circular networks with non-global coupling by performing extensive simulations. The general algorithm implemented in this step allowed for the investigation of arbitrary graphs, and thus it was used to investigate small-world graphs, which were generated from these same circular graphs. At the same time, a mean-field approximation for small-world networks was introduced, which predicts the stability of travelling waves at positive coupling regimes, where usually the globally synchronized solution would be observed. The limit of rewiring probability $p = 0$ recovers the mean field approximation proposed in previous works, but travelling waves were predicted to be stable even when the underlying graph has some disorder. These wave solutions compete with global oscillations as well as with each other when there is more than one stable wave number, leading to spontaneous creation and annihilation of wave numbers m. Finite systems will always be subject to these fluctuations in wave number, but larger systems are more robust since noise becomes smaller relative to system size at the wave boundaries. For example in figure 28 we see stable waves for $N = 16000$ even though $p = 0.0128$ consists of a relatively large amount of disorder.

Initial simulations and scaling analyses indicated that wave solutions did not lose stability if the interaction range and system size increase proportionally to each other, a property captured by the MF approximation. To further probe the validity of such an approximation, we tested other predictions, such as the stability of wave solutions even with disorder due to rewiring with probability p, and also verified that the speed of propagation should increase with increasing natural frequencies.

With ongoing studies in mind, there are threads that could still be unwound. An interesting simulation that hasn't been performed yet would investigate how travelling waves behave when reaching a discontinuous step in the natural frequencies, perhaps creating a reflected wave or a series of defects as each region oscillates with a different synchronized frequency.

A more theoretical and perhaps more profound ramification is the possible connection between non-equilibrium coupled oscillators and topological phase transitions of the Kosterlitz-Thouless type, which were hinted at on initial works by Wood et al. [1] and other independent researchers with whom I've had the opportunity to discuss this work. This speculation is based on the spatial clustering exhibited by such systems, not only on circular graphs, where we have seen such spatial clustering and also defect structures, but also on the 2d square lattice in early studies of the cyclic models.

Bibliography

[1] K. Wood, C. Van den Broeck, R. Kawai, and K. Lindenberg, "Universality of synchrony: Critical behavior in a discrete model of stochastic phase-coupled oscillators," *Phys. Rev. Lett.*, vol. 96, no. 14, p. 145701, 2006. Cited 10 time(s) on pages 14, 24, 25, 27, 28, 30, 46, 58, 62, and 71.

[2] J. D. da Fonseca and C. V. Abud, "The kuramoto model revisited," *J. Stat. Mech. Theory Exp.*, vol. 2018, p. 103204, oct 2018. Cited on page 15.

[3] A. Jeffrey and D. Zwillinger, *Table of integrals, series, and products*. Elsevier, 2007. Cited on page 20.

[4] K. L. Rodrigues and R. Dickman, "Synchronization of discrete oscillators on ring lattices and small-world networks," *J. Stat. Mech. Theory Exp.*, vol. 2020, no. 4, p. 043406, 2020. Cited 4 time(s) on pages 24, 53, 58, and 62.

[5] Y. Kuramoto, *Chemical oscillations, waves, and turbulence*. Courier Corporation, 2003. Cited 2 time(s) on pages 24 and 27.

[6] S. H. Strogatz and I. Stewart, "Coupled oscillators and biological synchronization," *Sci. Am.*, vol. 269, no. 6, pp. 102–109, 1993. Cited on page 24.

[7] S. H. Strogatz, "From kuramoto to crawford: exploring the onset of synchronization in populations of coupled oscillators," *Phys. D: Nonlinear Phenom.*, vol. 143, no. 1-4, pp. 1–20, 2000. Cited 2 time(s) on pages 24 and 27.

[8] S. H. Strogatz, *Sync: How order emerges from chaos in the universe, nature, and daily life*. Hachette UK, 2012. Cited on page 24.

[9] A. Pikovsky, M. Rosenblum, and J. Kurths, *Synchronization: a universal concept in nonlinear sciences*, vol. 12. Cambridge university press, 2003. Cited on page 24.

[10] K. I. Tainaka, "Lattice model for the lotka-volterra system," *J. Phys. Soc. Jpn.*, vol. 57, no. 8, pp. 2588–2590, 1988. Cited on page 24.

[11] K. I. Tainaka, "Stationary pattern of vortices or strings in biological systems: lattice version of the lotka-volterra model," *Phys. Rev. Lett.*, vol. 63, no. 24, p. 2688, 1989. Cited on page 24.

[12] K. Tainaka and Y. Itoh, "Topological phase transition in biological ecosystems," *EPL (Europhysics Lett.*, vol. 15, no. 4, p. 399, 1991. Cited on page 24.

[13] Y. Itoh and K. I. Tainaka, "Stochastic limit cycle with power-law spectrum," *Phys. Lett. A*, vol. 189, no. 1-2, pp. 37–42, 1994. Cited on page 24.

[14] K. I. Tainaka, "Vortices and strings in a model ecosystem," *Phys. Rev. E*, vol. 50, no. 5, p. 3401, 1994. Cited on page 24.

[15] K. Wood, C. Van den Broeck, R. Kawai, and K. Lindenberg, "Critical behavior and synchronization of discrete stochastic phase-coupled oscillators," *Phys. Rev. E*, vol. 74, no. 3, p. 031113, 2006. Cited 3 time(s) on pages 24, 58, and 62.

[16] K. Wood, C. Van den Broeck, R. Kawai, and K. Lindenberg, "Effects of disorder on synchronization of discrete phase-coupled oscillators," *Phys. Rev. E*, vol. 75, no. 4, p. 041107, 2007. Cited on page 24.

[17] K. Wood, C. Van den Broeck, R. Kawai, and K. Lindenberg, "Continuous and discontinuous phase transitions and partial synchronization in stochastic three-state oscillators," *Phys. Rev. E*, vol. 76, no. 4, p. 041132, 2007. Cited 2 time(s) on pages 24 and 58.

[18] V. R. Assis, M. Copelli, and R. Dickman, "An infinite-period phase transition versus nucleation in a stochastic model of collective oscillations," *J. Stat. Mech. Theory Exp.*, vol. 2011, no. 09, p. P09023, 2011. Cited 8 time(s) on pages 25, 27, 28, 29, 30, 36, 46, and 62.

[19] D. Escaff, K. Lindenberg, *et al.*, "Arrays of stochastic oscillators: Nonlocal coupling, clustering, and wave formation," *Phys. Rev. E*, vol. 90, no. 5, p. 052111, 2014. Cited 13 time(s) on pages 25, 33, 35, 36, 37, 44, 46, 47, 48, 55, 56, 58, and 61.

[20] Y. Kuramoto, T. Aoyagi, I. Nishikawa, T. Chawanya, and K. Okuda, "Neural network model carrying phase information with application to collective dynamics," *Prog. Theor. Phys.*, vol. 87, no. 5, pp. 1119–1126, 1992. Cited on page 27.

[21] H. Ohta and S. I. Sasa, "Critical phenomena in globally coupled excitable elements," *Phys. Rev. E*, vol. 78, no. 6, p. 065101, 2008. Cited on page 27.

[22] S. Shinomoto and Y. Kuramoto, "Phase transitions in active rotator systems," *Prog. Theor. Phys.*, vol. 75, no. 5, pp. 1105–1110, 1986. Cited on page 27.

[23] F. Rozenblit and M. Copelli, "Collective oscillations of excitable elements: order parameters, bistability and the role of stochasticity," *J. Stat. Mech. Theory Exp.*, vol. 2011, no. 01, p. P01012, 2011. Cited on page 27.

[24] K. Huang, "Statistical mechanics, 2nd," *Ed. (New York: John Wiley & Sons)*, 1987. Cited on page 28.

[25] M. Plischke and B. Bergersen, *Equilibrium Statistical Physics*. World Scientific, 1994. Cited on page 30.

[26] D. J. Watts and S. H. Strogatz, "Collective dynamics of 'small-world'networks," *Nature*, vol. 393, no. 6684, p. 440, 1998. Cited 2 time(s) on pages 37 and 38.

Appendix

APPENDIX A – Path length and clustering for regular ring lattices

A.1 Average Path Length

The distance L_{ij} between two nodes i and j is the minimum number of edges that must be traversed to connect them. The average path length is defined as the average distance between every possible pair of nodes in the network. For a network with N nodes this is:

$$L = \frac{2}{N^2 - N} \sum_{i<j} L_{ij} \tag{A.1}$$

Consider the lowest node in a ring graph with N nodes and $2K$ neighbors per node. Going counterclockwise (CCW), there are K nodes at distance 1, then K nodes at distance 2 and so on until we reach some region near the top. In total, there will be G groups of nodes, each with K nodes, at distances $1, 2, 3..., G$ from our starting point at the bottom. G is given by the largest integer smaller than $(N-1)/(2K)$. This can be written with the floor operation:

$$G = \left\lfloor \frac{N-1}{2K} \right\rfloor \tag{A.2}$$

This same procedure can be performed from the clockwise (CW) direction. Thus, there are $2K$ nodes at distance 1 and so on up to distance G. The last group of nodes at the top is therefore at a distance $G+1$, but it contains less than $2K$ nodes. Indeed, it contains a number R of nodes equal to the remainder of the integer division of $N-1$ by $2K$:

$$R = N - 1 - 2KG \tag{A.3}$$

This reasoning can be visualized in Fig. 29.

Since there are $N-1$ pairs between the bottom node and all other nodes in the lattice, the average distance L_0 between the bottom node and all other nodes is then given by:

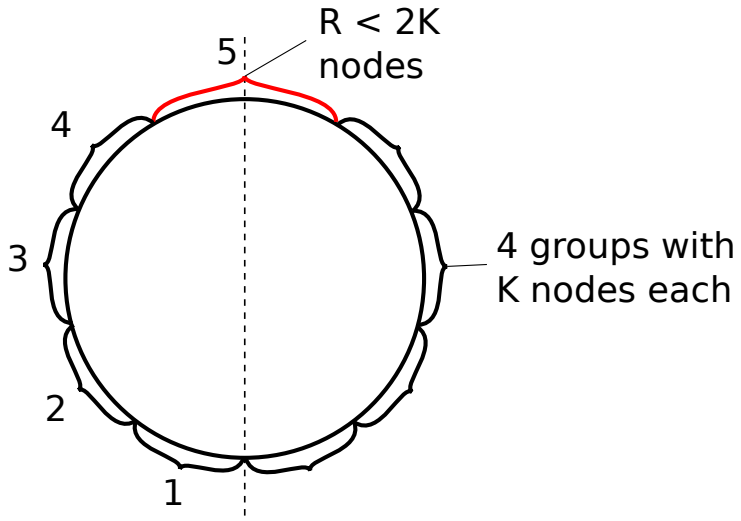

Figure 29 – Counting the number of nodes at distances visually. Here $G = 4$ groups at distances $1, 2, 3, 4$ from the bottom node.

$$\begin{aligned} L_0 &= \frac{1}{N-1}\left[2K\sum_{i=1}^{G} i + R(G+1)\right] \\ &= \frac{1}{N-1}\left[KG(G+1) + R(G+1)\right] \\ L_0 &= (G+1)\left(1 - \frac{KG}{N-1}\right) \end{aligned} \tag{A.4}$$

where we used equation A.3 to substitute in for R. Because we started with an arbitrary node at the bottom, this result is true for any given node in a regular ring, and thus we conclude that the average path length for the whole network is just L_0.

$$\begin{aligned} L(N,K) &= (G+1)\left(1 - \frac{KG}{N-1}\right) \\ \text{with} \qquad G &= \left\lfloor \frac{N-1}{2K} \right\rfloor \end{aligned} \tag{A.5}$$

A.2 Average Clustering

The clustering coefficient for a node i in the graph is defined as: let n_i be the number of neighbors of some node i. Then, there are at most $(n_i^2 - n_i)/2$ connections between any two of its neighbors. Let m_i be the number of actual connections that are present in a particular graph. Then, the clustering coefficient C_i of node i is given by:

$$C_i = \frac{2m_i}{n_i^2 - n_i} \tag{A.6}$$

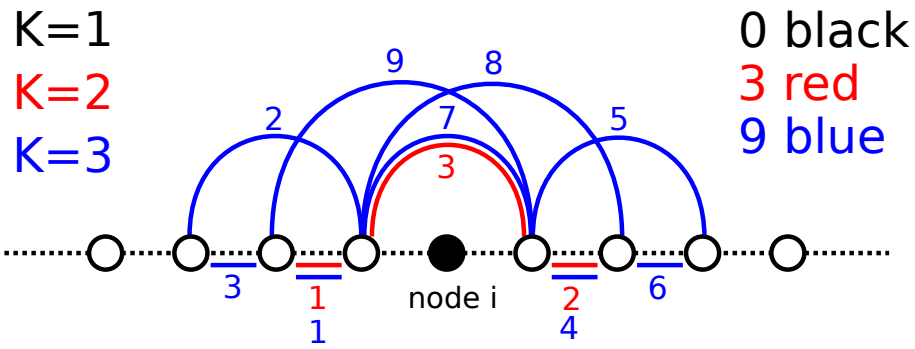

Figure 30 – (Color online) Counting m for $k = 1, 2, 3$. We note three contributions to m: a fully connected group of K CW neighbors (left), a fully connected group of K CCW neighbors (right) and connections that go "over" the center node.

If there are N nodes in the graph, the average clustering coefficient is thus given by:

$$C = \frac{1}{N}\sum_{i=1}^{N} C_i \tag{A.7}$$

First, consider a "close-up" of a section of a regular ring where $N \gg K$. Consider a node i with K CW neighbors and K CCW neighbors. Let m be the number of connections between neighbors of node i. We can manually count m for some values of K:

$$\begin{aligned} m &= 0 \quad \text{if} \quad K \leq 1 \\ m &= 3 \quad \text{if} \quad K = 2 \\ m &= 9 \quad \text{if} \quad K = 3 \end{aligned}$$

The general case for $N \gg K$ can be counted by summing the contributions of the three groups as shown in figure 30. Two fully connected groups of K nodes each contributes with $(K^2 - K)$ connections. The connections that bypass node i also contribute with $(K^2 - K)/2$ connections and thus we have.

$$m = \frac{3}{2}(K^2 - K) \tag{A.8}$$

Now we divide equation A.8 by the total number of connections between the $2K$ neighbors of node i to get its clustering coefficient C_i:

$$C_i(N, K) = \frac{3K - 3}{4K - 2} \tag{A.9}$$

When N is not so large compared to K, additional connections between the CCW and CW neighbors may appear by looping around the opposite side of node i, as depicted in

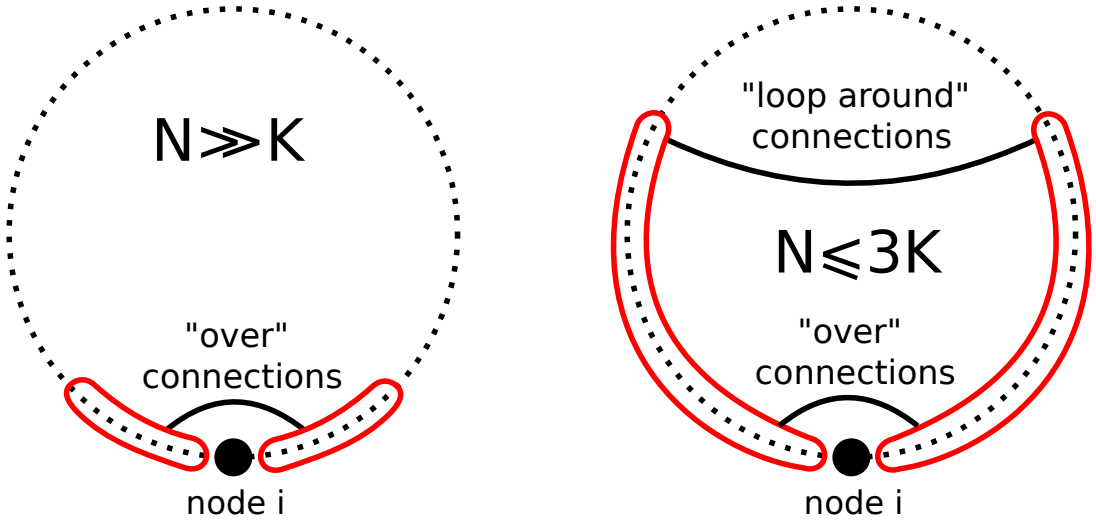

Figure 31 – Connections that contribute to the clustering coefficient of node i. The red regions represent the CW and CCW groups of neighbors of node i, and they are fully connected each within itself. Additional connections are made going "over" node i, but when $N \leq 3K$ there are additional connections that loop around the opposite side of the lattice.

figure 31. These additional connections will be present whenever the remaining nodes that are neither in the CW or CCW group are fewer than K. The number of such nodes is just $N - 2K - 1$, which gives us the condition $N \leq 3K$ for additional connections to be present.

The number of "loop around" connections that will be present will depend on how many nodes there are in the remaining group after removing node i and its immediate neighbors. Let this number be denoted by $D = N - 2K - 1$. Then, the number of additional connections will be given by

$$(K - D) + (K - D - 1) + ... + 2 + 1 = \frac{(K - D + 1)(K - D)}{2} \tag{A.10}$$

Adding equation A.10 to A.8 we get

$$m = \frac{3}{2}(K^2 - K) + \frac{1}{2}(3K - N + 1)(3K - N + 2) \tag{A.11}$$

And thus the clustering now becomes:

$$C_i(N, K) = \frac{3K - 3}{4K - 2} + \frac{(3K - N + 1)(3K - N + 2)}{4K^2 - 2K} \tag{A.12}$$

This formula holds up to the point when $D = 0$ or $N = 2K + 1$. For all values $D \leq 0$ the regular ring is in fact a complete graph, where every node connects to every

other. In these cases the clustering coefficient is always equal to one. Formulas A.9 and A.12 together offer a complete expression for the clustering of node i. Since $C_i = C_j \quad \forall i, j$, this is just the average clustering of the whole network and we finally get:

$$C(N,K) = \begin{cases} \frac{3K-3}{4K-2} & \text{if} \quad N > 3K \\ \frac{3K-3}{4K-2} + \frac{(3K-N+1)(3K-N+2)}{4K^2-2K} & \text{if} \quad 3K \geq N > 2K+1 \\ 1 & \text{else} \end{cases} \tag{A.13}$$